Analytical Approximation to the Scheutjens−Fleer Theory for Polymer Adsorption from Dilute Solution. 2. Adsorbed Amounts and Structure of the Adsorbed Layer

G. J. Fleer* and J. van Male

Laboratory for Physical and Colloid Science, Agricultural University, Wageningen, Dreijenplein 6, 6703 HB Wageningen, The Netherlands

A. Johner

Institut Charles Sadron, 6 rue Boussingault, 67083 Strasbourg Cedex, France

Received May 19, 1998; Revised Manuscript Received November 10, 1998

ABSTRACT: In part I we adapted the recent analytical mean-field theory of polymer adsorption by Semenov et al. to match the numerical lattice theory of Scheutjens and Fleer (SF). Here we calculate explicitly the contributions of trains, loops, and tails to the adsorbance and their size distributions. We choose conditions in the so-called plateau region, which is most relevant from an experimental point of view. We thus use the "plateau approximation", where the two simultaneous equations that determine the proximal length p and the distal length d can be uncoupled. The variations with bulk concentration, chain length, and surface affinity compare quite nicely with the SF numerics. Both a good solvent (at the mean-field level) and Θ solvent are considered; the agreement is better in the former case.

1. Introduction

In the first paper of this series,[1] we described an adaptation of the continuum mean-field theory originally proposed by Semenov et al.[2] that we designed to match the mean-field lattice theory of Scheutjens and Fleer.[3−5] As in the original continuum theory, the layer is described by two order parameter fields, called $g(z)$ and $f(z)$. The former is defined as the classical ground-state eigenfunction in the actual molecular potential and measures the statistical weight of an adsorbed chain ending at z (up to free state corrections). The latter describes the statistical weight of a tail section dangling beyond z. We argue that for moderate chain lengths and/or high dilution the tail contribution to the monomer concentration is a small correction up to the dilute layer edge where the molecular field is irrelevant anyhow, the edge being essentially ruled by the bulk chemical potential.[6] This is in contrast with the asymptotic limit of infinitely long chains,[2] where the crossover from loop to tail dominance is in the semidilute part of the layer unless the bulk is exponentially dilute. We already showed[1] that in practice the perturbative tail treatment is accurate over a wide range of concentrations.

Our treatment further differs from the original one by the applied boundary condition, which is transposed from the lattice theory.[1] This allows for a specific treatment of the monolayer in direct contact with the wall where detailed interaction energies can be used. Further from the wall the interaction potential is expanded in powers of the monomer density, and only the lowest order is retained. Altogether this treatment explicitly introduces an adsorption threshold (which is model-dependent) and gives back the universal (mean-field) behavior close to the threshold. At high surface affinities, the surface concentration is found to saturate.

Our treatment applies to both good solvents (at the mean-field level and up to $\chi \approx 0.47$) and a Θ solvent ($\chi = 0.5$). The agreement between the numerics and the analytical model was already found to be better for good solvents from the few results presented in part I. From a fundamental point of view, the theory incorporates the lowest-order free state correction[2,7] to the loop concentration in a good solvent but not in a Θ solvent. Correcting for that does hardly improve the Θ results. The main discrepancy stems from the markedly higher densities, as compared to a good solvent, outside the first layer and from the neglect of the nonlocal energy contributions in the continuum theory. When these are disregarded, the linear term in the expansion of the potential as a function of the monomer concentration cancels exactly in a Θ solvent, and the much smaller quadratic contribution is the leading term. However, when nonlocal energy effects are included, as in the lattice model, the linear term is *over*compensated and the field is even smaller.

In this paper we systematically study the variations of the total adsorbance and its decomposition in contributions due to trains, loops, and tails and the size distribution of these sequences as a function of concentration, chain length, and surface affinity. In all cases the derived analytical expressions are at least in fair agreement with the numerics.

This paper contains three appendices. The first two deal with loop and tail size distributions, and the third gives a supplement to the list of symbols (compare Appendix 1 of paper I).

2. Theory

2.1. General. In part I the complete set of equations for the analytical approximations was given. We will not repeat these equations but summarize a few important results. Moreover, we use only those approximations that are relevant for the plateau regime, where the train density is of order unity. Consequently, we will drop the subscript p as used in sections 4.3.2 and 4.3.3 of paper I. We consider two extreme cases for the solvency: $\chi = 0$ and $\chi = 0.5$. Hence, the "good solvent" equations in this paper are simpler versions of the more

10.1021/ma980794q CCC: $18.00
Published on Web 01/22/1999

general ones in paper I, obtained by substituting $\chi = 0$.

Trains and loops are described by the ground-state eigenfunction $g(z)$, which depends on the distance z from the surface and contains two parameters: the proximal length p and the distal length d. In the plateau region, the first is only a function of the adsorption energy parameter χ_s, as described in eqs 45 and 47 of part I. We repeat these important equations (with for the good solvent only the special case $\chi = 0$):

$$e^{-\chi_s} = \left(1 - \frac{q^2}{{p_1}^2}\right)\left(\lambda_0 + \frac{\lambda}{1 + 1/p_1}\right) \qquad q \equiv p_\infty + \frac{1}{2} = \sqrt{2\lambda} \quad (1g)$$

$$e^{-\chi_s - \lambda/2} = \left(1 - \frac{q}{p_1}\right)\left(\lambda_0 + \frac{\lambda}{\sqrt{1 + 1/p_1}}\right) \times \exp\left[\left(\lambda_0 + \frac{\lambda}{(1 + 1/p_1)}\right)\frac{q}{p_1}\right] \qquad q \equiv p_\infty + \frac{1}{2} = \frac{\sqrt{6\lambda}}{2} \quad (1t)$$

where $p_1 = p + {}^1/_2$ (see eq 3c). For the high-χ_s limit $p_{1,\infty} = p_\infty + {}^1/_2$ we use the symbol q. The lattice parameter λ equals ${}^1/_4$ for a hexagonal lattice and ${}^1/_6$ for a cubic lattice, and $\lambda_0 = 1 - 2\lambda$. Throughout this paper, we will give results for both solvencies in one equation, where the first form is indicated with g (good solvent; in this paper only $\chi = 0$) and the second with t (Θ). The solution of eq 1 is shown in Figure 6 of part I, and approximate explicit expressions for p were derived in paper I. The proximal length p diverges at the critical adsorption χ_{sc}. In a good solvent and for $\lambda = {}^1/_4$, $\chi_{sc} = -\ln(1 - \lambda) = 0.288$; the proximal length p equals 0.595 at $\chi_s = 1$ and it reaches a constant level $p_\infty = q - {}^1/_2 = 0.207$ at high χ_s. In a Θ solvent $\chi_{sc} = -\ln(1 - \lambda) - \lambda\chi = 0.163$ for $\lambda = {}^1/_4$, and p is smaller: $p = 0.396$ at $\chi_s = 1$, and $p_\infty = q - {}^1/_2 = 0.112$ at high χ_s.

The distal length d depends mainly on the chain length N and the solution concentration φ^b. As in paper I, we use the concentration parameter y, defined by $y^2 = \ln(1/\varphi^b)$. A first-order estimate d_0 for the distal length is

$$d_0 = \frac{\sqrt{\lambda N}}{y} \qquad (2)$$

As we will see below, d is slightly above d_0, typically by 10% or 20%; the correction depends on all three parameters N, φ^b (or y), and χ_s (or p).

The distance z from the surface is defined such that the surface is situated at $z = 0$ and that the center of the lattice layers in the numerical SCF model is at $z = 0.5, 1.5, \ldots$; train segments are thus at $z = 0.5$. It is convenient to introduce a normalized coordinate x and some specific values x_i of this parameter:

$$x = \frac{z + p}{d}, \quad x_i = \frac{p_i}{d}, \quad p_i = p + \frac{i}{2} \qquad (3a,b,c)$$

Clearly, at the surface ($z = 0$), $x = x_0 = p/d$. The value x_1 refers to the middle of the train layer, which is treated in a discrete way. The parameter x_2 corresponds to $z = 1$ and is the lower bound for the loop and tail region, where a continuum description is used in the analytical model. Tails start in the middle of the second layer, at $z = {}^3/_2$ or $x = x_3$.

The eigenfunction g, giving the end-point distribution of adsorbed chains, can be written as

$$g = \frac{q}{d \sinh x} \qquad g = \sqrt{\frac{2q}{d \sinh 2x}} \qquad (4g,t)$$

for a good solvent ($\chi = 0$) and a Θ solvent ($\chi = 0.5$), respectively. Note that q is not the same for both solvencies (see eq 1).

The concentration of trains, loops, and tails is described by

$$\varphi^{tr} = {g_1}^2, \quad \varphi^l = g^2 \ (z > 1), \quad \varphi^t = \frac{2b}{N} gf \qquad (5a,b,c)$$

where $g_1 = g(x_1)$. The function f is defined in eqs I-33 and I-37; it can be written in terms of the difference between a universal function $\gamma(x)$, which is plotted in Figure I-2a, and a nonuniversal correction $\gamma_2(x)$. In the present paper we concentrate on the main trends and in most cases neglect this correction term. Then f may be approximated as $f = (d^2/\lambda)\gamma$, where γ is defined in eqs I-33b and I-34 (good solvent) or eqs I-37b and I-38 (Θ solvent). The tail monomer concentration in a good solvent is thus approximately proportional to $\gamma_g/\sinh x$ (see Figure I-2b), which function reaches a maximum $m = 0.31$ at $x_m = 0.88$; its integral, needed for the contribution of tails to the adsorbance, is $I = 0.733$. In a Θ solvent the relevant function is $\gamma_t/\sqrt{\sinh 2x}$ (see Figure I-2b), with a maximum $m = 0.28$ at $x_m = 0.86$ and an integral $I = 0.606$. These numerical values will show up in the equations for tails given below.

The normalization factor b in eq 5c for the tail concentration is proportional to g_1 which, as we shall see below, is in the plateau regime basically only a function of χ_s (or p). We write $b = \alpha g_1$, where α is given by eqs I-46b and I-48b, respectively:

$$\alpha = \frac{1 + d \sinh^2 x_1(\coth x_2 - 1)}{1 + d \sinh x_1 \ln \coth(x_2/2)}, \qquad \alpha = \frac{1 + (d/2) \sinh 2x_1 \ln \coth x_2}{1 + d\sqrt{\sinh 2x_1}(K - \sqrt{2x_2})} \quad (6g,t)$$

where $K = 1.854$. In the full treatment, given in paper I, α and d follow from solving two implicit equations, but here we will use only the explicit approximation obtained by substituting $d = d_0$ in $b = \alpha g_1$. In principle, α depends on all three parameters N, φ^b, and χ_s. However, the dependencies on φ^b and χ_s are very weak, as shown in Figure 1 where α is plotted for the range $N = 10^2 - 10^4$ and for two values of φ^b (10^{-3} and 10^{-10}) and two values of χ_s (0.5 and 5). For most conditions, a reasonable estimate for the order of magnitude of α is $1 - 0.15 \log N$, which equation is never off by more than about 10% in this parameter range. We will use this approximation that α depends only on N just for discussing the trends in the results. For all the computations we use eq 6 with $d = d_0$ and $x_i = p_i/d_0$.

We can now find a reasonable approximation for d. According to eq I-30b d is given by $d^{-2} = {d_0}^{-2}(1 + 2y^{-2} \ln b)$, or $d^{-2} = (y^2 + 2 \ln b)/(\lambda N)$. Analogously to eq 2, we write

$$d = \frac{\sqrt{\lambda N}}{Y}, \quad Y^2 = y^2 + 2 \ln b = \ln\left(\frac{\alpha^2 \Gamma^{tr}}{\varphi^b}\right) \quad (7a,b)$$

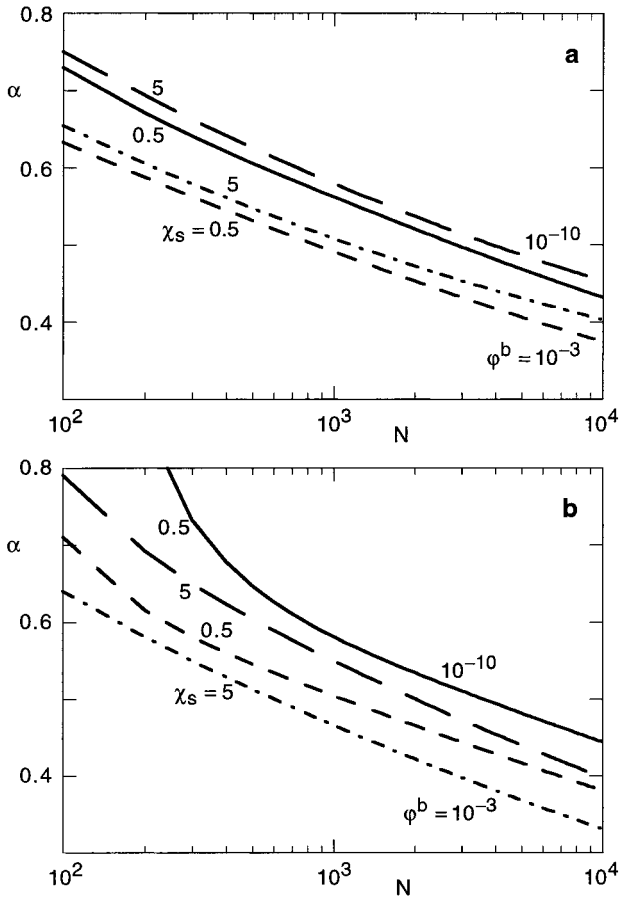

Figure 1. Dependence of the parameter α on N, for $\varphi^b = 10^{-3}$ and 10^{-10} and $\chi_s = 0.5$ and 5. Diagram a is for $\chi = 0$ and diagram b for $\chi = 0.5$. This figure was computed for $\lambda = 1/4$, but a plot for $\lambda = 1/6$ looks nearly the same.

where $\Gamma^{tr} = \varphi^{tr} = g_1^2$. The parameter Y depends mainly on φ^b, since the correction 2 ln b is small, but Y is slightly smaller than y because both α and Γ^{tr} are below unity. The magnitude of the correction depends on χ_s (through Γ^{tr}, see eq 8) and (weakly) on N (through $\alpha \approx 1 - 0.15 \log N$).

2.2. Adsorbed Amounts. We summarize the equations for the adsorbed amounts Γ^{tr}, Γ^l, and Γ^t in trains, loops, and tails, respectively. For trains and loops, we give both the full expressions for $\chi = 0$ (g) and $\chi = 0.5$ (t) (taken from paper I) as well as the limiting forms for long chains in the plateau regime; in the latter case $p/d << 1$, $x_1 << 1$, and $x_2 << 1$ so that $\sinh x = x + x^3/6$ and $\coth x = 1/x$. Then we have

$$\Gamma^{tr} = \frac{q^2}{d^2 \sinh^2 x_1} \approx \frac{q^2}{p_1^2}\left(1 - \frac{p_1^2}{3d^2}\right),$$

$$\Gamma^{tr} = \frac{2q}{d \sinh 2x_1} \approx \frac{q}{p_1}\left(1 - \frac{2p_1^2}{3d^2}\right) \quad (8g,t)$$

$$\Gamma^l = \frac{q^2}{d}(\coth x_2 - 1) \approx \frac{q^2}{p_2}\left(1 - \frac{p_2}{d}\right),$$

$$\Gamma^l = q \ln \coth x_2 \approx q \ln \frac{d}{p_2} \quad (9g,t)$$

$$\Gamma^t = \frac{2.07\alpha}{Y^2}\sqrt{\lambda\Gamma^{tr}}, \quad \Gamma^t = \frac{1.90\alpha}{Y^{5/2}}N^{1/4}\sqrt{\lambda\Gamma^{tr}} \quad (10g,t)$$

According to eq 8, Γ^{tr} for long chains depends only on χ_s; obviously the high χ_s limit is $\Gamma^{tr} = 1$, which defines the limiting value of p_1 through $p_1 = q$, where again $q^2 = 2\lambda$ ($\chi = 0$) or $2q^2 = 3\lambda$ ($\chi = 0.5$). For loops (eq 9), a difference shows up between $\chi = 0$ and $\chi = 0.5$ as to the chain-length dependence. In a good solvent and for long chains, Γ^l depends only on χ_s, basically as $1/p_2$; in the limit $\chi_s \to \infty$ we have $\Gamma^l = q^2/(q + 1/2)$, which gives 0.41 monolayers for $\lambda = 1/4$. In a Θ solvent Γ^l depends on χ_s as $\ln(1/p_2)$. A more important difference is the ln d dependence for $\chi = 0.5$, implying a increase of the adsorbed amount as log N, and a very weak increase with the bulk solution concentration as $\ln(1/Y) \approx -1/2 \ln(\ln(1/\varphi^b))$.

The equations for tails (eq 10) were obtained from $\Gamma^t = (2b/N)I_{gf}$, using $I = 0.733$ ($\chi = 0$) and $I = 0.606$ ($\chi = 0.5$) as discussed above. In a good solvent Γ^t is mainly determined by φ^b ($\Gamma^t \propto Y^{-2} \approx 1/\ln(1/\varphi^b)$), although there is a weak χ_s dependence (through Γ^{tr}) and a slight dependence on N (through α). In a Θ solvent, the concentration dependence is somewhat stronger ($\propto Y^{-5/2}$), and Γ^t now increases weakly with N ($\propto N^{1/4}$). It is worth noting that the tail fraction $\nu^t = \Gamma^t/\Gamma$, where $\Gamma = \Gamma^{tr} + \Gamma^l + \Gamma^t$, depends only very weakly on N.

2.3. Structural Aspects. According to eqs 4 and 5, the concentration profile of loops is a monotonously decreasing function of z, which for $z > d$ falls off exponentially, with a decay length d for the eigenfunction g and, hence, a decay length $d/2$ for $\varphi^l = g^2$. The distance z_l where the loop concentration becomes equal to φ^b is found from $g^2(x_l) = \varphi^b$, or $z_l = dx_l - p$, with

$$x_l \approx \frac{1}{2}\ln\left(\frac{4q^2}{\varphi^b d^2}\right) = \frac{1}{2}\left(y^2 + 2\ln\frac{2q}{d}\right),$$

$$x_l \approx \frac{1}{2}\ln\left(\frac{4q}{\varphi^b d}\right) = \frac{1}{2}\left(y^2 + 2\ln\frac{4q}{d}\right) \quad (11g,t)$$

where we assumed $\sinh x = e^x/2$. The leading term in these expressions is $\ln(1/\varphi^b) = y^2$: $x_l \approx y^2/2$ or $z_l \approx 1/2 y\sqrt{\lambda N}$.

In a similar way the distance z_t where the tail concentration equals φ^b can be found. We may take for the function f its limiting value d^2/λ so that according to eq 5c and 7a $\varphi^t = 2bg/Y^2$. Now $z_t = dx_t - p$ is found from

$$x_t \approx \ln\left(\frac{4\alpha q\sqrt{\Gamma^{tr}}}{\varphi^b Y^2 d}\right) \approx y^2 + \ln\left(\frac{4\alpha q^2}{Y^2 d p_1}\right),$$

$$x_t \approx \ln\left(\frac{4\alpha\sqrt{q\Gamma^{tr}}}{\varphi^b Y^2\sqrt{d}}\right) \approx y^2 + \ln\left(\frac{4\alpha q}{Y^2\sqrt{d p_1}}\right) \quad (12g,t)$$

Hence, x_t is around y^2, or $z_t \approx y\sqrt{\lambda N}$, roughly twice z_l.

At shorter distances φ^t passes through a maximum at $x_m = 0.88$ ($\chi = 0$) or $x_m = 0.86$ ($\chi = 0.5$). Therefore,

$$z_m = 0.88d - p, \quad z_m = 0.86d - p \quad (13g,t)$$

The value φ_m at this maximum is given by

$$\varphi_m = \frac{0.88\alpha}{Y}\sqrt{\frac{\Gamma^{tr}}{N}}, \quad \varphi_m = \frac{0.88\alpha}{Y^{3/2}}\sqrt{\frac{\Gamma^{tr}}{N^{1/4}}} \quad (14g,t)$$

where the numerical factors are $0.31 \times 2\sqrt{2}$ and $0.28 \times 2 \times 6^{1/4}$, respectively; the numbers 0.31 and 0.28

correspond to the height of the maximum in the normalized tail profiles in Figure I-2b.

In the theory by Semenov et al.,[2] the crossover distance z^* between the loop-dominated inner part of the layer and the tail-dominated outer part plays an important role. The central assumption in the ground-state solution for g and f is that $\epsilon + u$ (where $\epsilon = \lambda/d^2$) equals $\epsilon + \varphi$ ($\chi = 0$) or $\epsilon + \varphi^2/2$ ($\chi = 0.5$). In our present analytical approach we replace φ by φ^l, which is only correct for the loop-dominated regime ($z \lesssim z^*$). On the other hand, only in the region $z \lesssim d$ the precise value of u is important: in the distal regime $\epsilon + u$ may be replaced by ϵ. For the validity of our approach it is thus necessary that the loop-dominated regime extends at least to the distal length: z^* should be larger than d.

We calculate z^* from the intersection of the loop and tail profiles: $g^2 = (2b/N)gf$. According to eqs I-33a and 37a, $f \approx (d^2/\lambda N)\gamma$ where, for large z, γ may be replaced by $1 - (\pi^2/4)e^{-x}$ ($\chi = 0$) or by $1 - (K/\sqrt{2})e^{-x}$ ($\chi = 0.5$). Using $d^2/\lambda N = Y^{-2}$ (eq 7) we find z^* from $g = (2b/Y^2)\gamma$, where in g we use $\sinh x = e^x/2$. The result is $z^* = dx^* - p$, where x^* is given by

$$x^* = \ln\left(\frac{\pi^2}{4} + \frac{Y^2}{b}\frac{q}{d}\right) \approx \ln\left(\frac{\pi^2}{4} + \frac{Y^2}{\alpha}\frac{p_1}{d}\right),$$
$$x^* = \ln\left(\frac{K}{\sqrt{2}} + \frac{Y^2}{b}\sqrt{\frac{q}{d}}\right) \approx \ln\left(\frac{K}{\sqrt{2}} + \frac{Y^2}{\alpha}\sqrt{\frac{p_1}{d}}\right) \quad (15g,t)$$

2.4. Number and Length of Trains, Loops, and Tails. The GSA approach does also provide relatively simple expressions for the number of trains, loops, and tails per adsorbed chain. We first summarize the exact equations for the SCF lattice model.[4,5] These are

$$n^{tr}(s) = \frac{2(\lambda_0 G_1)^s N-s}{\lambda_0 G_N^a}\sum_{t=0} G_{2,t}G_{2,N-s-t}, \quad n^{tr} = \sum_{s=1}^{N} n^{tr}(s) \quad (16a,b)$$

$$n^l(s) = \frac{\lambda^2 G^t_{2,s}}{G_N^a}\sum_{t=2}^{N-s-1} G^a_{1,t}G^a_{1,N-s-t},$$
$$n^l = n^{tr} - 1 = \frac{\lambda}{G_N^a}\sum_{s=2}^{N-1} G^a_{2,s}G^a_{1,N-s} \quad (17a,b)$$

$$n^t(s) = \frac{2\lambda}{G_N^a}G^f_{2,s}G^a_{2,N-s}, \quad n^t = \sum_{s=1}^{N-1} n^t(s) = 2\left(1 - \frac{G^a_{1,N}}{G_N^a}\right) \quad (18a,b)$$

In these expressions, $n^x(s)$ is the number of trains, loops, or tails of length s per chain, and n^x is the total number of these sequences per chain. The parameter $G_1 = e^{-u_1}$ is the weighting factor for adsorbed segments, and $\lambda_0 = 1 - 2\lambda$. The quantities $G_{z,s}$, $G^a_{z,s}$, and $G^f_{z,s}$ are the end-point distributions of all chains, of the adsorbed chains, and of the free chains, respectively; they are given in eqs 1−6 of paper I. In eq 16a $G_{2,0}$ is defined formally as $1/\lambda$. The quantity G_N^a is the sum of $G^a_{z,N}$ over all layers (eq I-9b); it is equal to Γ/φ^b (eq I-9a). In eq 17a, $G^t_{z,s}$ is the tail end-segment distribution,[4,5] giving the statistical weight of tails of s segments long to end in layer z. For the loop distribution we need only $G^t_{2,s}$ because a loop is a tail ending in the second layer. The set $G^t_{z,s}$ is computed from the propagator relation I-2, with the starting condition $G^t_{z,1} = G_z\delta_{z-2}$ (so that $G^t_{2,1} = G_2$ is the only nonzero element of the vector $G^t_{z,1}$); moreover, $G^t_{1,s}$ has to be set zero for any s.

The average length of trains, loops, and tails is given by

$$l^{tr} = N\nu^{tr}/n^{tr}, \quad l^l = N\nu^l/n^l, \quad l^t = N\nu^t/n^t \quad (19a,b,c)$$

where $\nu^{tr} = \Gamma^{tr}/\Gamma$, $\nu^l = \Gamma^l/\Gamma$, and $\nu^t = \Gamma^t/\Gamma$.

The above discrete expressions may be transformed into their continuum analogues by substituting $G^a_{z,s} \approx b^{-1}g(z)e^{\epsilon s}$ (eq I-14) and approximating $G_{2,s} \approx G^a_{2,s}$. We first consider the averages and start with the trains. The sum in eq 16a becomes $b^{-2}g_2^2(N - s)e^{\epsilon(N-s)}$, so that $n^{tr}(s) = A^{tr}(N - s)(e^{-\epsilon}\lambda_0 G_1)^s$; we analyze this expression in more detail in the following section (eq 24). The prefactor A^{tr} is given by $A^{tr} = \lambda^2\lambda_0^{-1}g_2^2/\Gamma$ since $G_N^a = \Gamma/\varphi^b$ and $b^{-2}\varphi^b e^{\epsilon N} = 1$. According to the boundary condition at the surface (eq I-28), the product $e^{-\epsilon}\lambda_0 G_1 = \lambda_0 e^{-(\epsilon+u_1)}$ equals $\lambda_0/(\lambda_0 + \lambda g_2/g_1)$. Now n_{tr} is found from eq 16b, and l^{tr} follows as $\sum s n^{tr}(s)/\sum n^{tr}(s)$. For convenience, we write $n^{tr}(s) = A^{tr}Nr^s$, with $1/r = 1 + \lambda g_2/(\lambda_0 g_1)$; we replace $N - s$ by N, which induces no appreciable error in l^{tr} and n^{tr} since most of the trains are small. For the sums we use $\sum r^s = r(1 - r)^{-1}$ and $\sum s r^s = r(1 - r)^{-2}$. The result for trains is

$$\frac{n^{tr}}{N} = \frac{\lambda g_1 g_2}{\Gamma} = \lambda\nu^{tr}\frac{g_2}{g_1}, \quad l^{tr} = 1 + \frac{\lambda_0}{\lambda}\frac{g_1}{g_2} \quad (20a,b)$$

The number n^l of loops per chain is nearly equal to the number n^{tr} of trains (in the exact lattice model $n^{tr} = n^l + 1$). Indeed, eq 17b with $G^a_{z,s} \approx b^{-1}ge^{\epsilon s}$ leads to the same expression as given in eq 20a. The average loop length follows from eqs 19b and 20a:

$$n^l \approx n^{tr}, \quad l^l = \frac{\Gamma^l}{\lambda g_1 g_2} = \frac{1}{\lambda}\frac{\nu^l}{\nu^{tr}}\frac{g_1}{g_2} \quad (21a,b)$$

The number of tails follows directly from eq 18b: $n^t = 2(1 - bg_1/\Gamma)$. The adsorbed amount Γ can also be written as $\Gamma = b(g_1 + I_g)$ (eq I-19), where the integral I_g is defined as $I_g = \int_1^\infty g\,dz$ (eqs I-35 and I-40). Hence, n^t is also given by $n^t = 2bI_g/\Gamma$. Substitution of this result in eq 19c, using $\Gamma^t = (2b/N)I_{gf}$ (where $I_{gf} = \int_1^\infty gf\,dz$), gives l^t as the ratio of two integrals:

$$n^t = 2\left(1 - \frac{bg_1}{\Gamma}\right) = 2(1 - \alpha\nu^{tr}), \quad l^t = \frac{I_{gf}}{I_g} \quad (22a,b)$$

We note that these equations are necessarily approximations; in the results section we will see that the error is typically of the order of 10% or 20% as compared to the numerical data. Also, the equations are not fully consistent. For example, both n^{tr} and l^{tr}, which were derived from eq 16, turn out to be too low. Consequently, eq 19a is not satisfied. For loops and tails, the analogous expressions 19b and 19c were used to find l^l and l^t; in this way the rather complicated expressions for the loop and tail size distributions (see following section) can be avoided.

In eqs 20 and 21, the ratio g_1/g_2 may be replaced by $\sinh x_3/\sinh x_1 \approx 1 + 1/p_1$ for $\chi = 0$ and by $\sqrt{\sinh 2x_3/\sinh 2x_1} \approx \sqrt{1+1/p_1}$ for $\chi = 0.5$, respectively.

Hence, this ratio is virtually only a function of χ_s, is of order (but above) unity, and reaches a maximum level for $\chi_s \rightarrow \infty$. For $\chi = 0$, this maximum value is $1 + 1/q$, which is 2.41 for $\lambda = {}^1/_4$. For $\chi = 0.5$, the maximum ratio is $\sqrt{1+1/q}$ or 1.62 for $\lambda = {}^1/_4$. Therefore, the train length l^{tr} is small: it can be written as $1 + \beta\lambda_0/\lambda$ (which is $1 + 2\beta$ for $\lambda = {}^1/_4$), where β is around 2.4 (or lower) at $\chi = 0$ and around 1.6 (or lower) at $\chi = 0.5$. According to eqs 19a and 19b, the loop length is the train length times ν^l/ν^{tr}. Hence, loops are smaller than trains in a good solvent (where trains dominate) and longer than trains in a Θ solvent (where $\nu^l/\nu^{tr} > 1$ in the plateau region). Because of the small train and loop lengths, the number of trains and loops per chain is large and approximately proportional to the chain length N.

The number of tails per chain can, obviously, never exceed 2. For $\chi = 0.5$, where ν^{tr} is relatively small, n^t is closer to 2 than for $\chi = 0$; in both cases n^t increases (slowly) with increasing N because both α and ν^{tr} decrease with N. In order to see the behavior of the tail length, we have to evaluate the ratio I_{gf}/I_g. Using again the approximations $I = 0.733$ for $\chi = 0$ and $I = 0.606$ for $\chi = 0.5$ for the integral $I \propto I_{gf}$, we find

$$l^t = \frac{0.73N}{Y^2 \ln \coth(x_2/2)}, \quad l^t = \frac{0.61N}{Y^2(K - \sqrt{2x_2})} \qquad (23g,t)$$

Hence, the tail length is roughly proportional to N and approximately inversely proportional to $\ln(1/\varphi^b)$. In a good solvent the logarithmic factor, containing $\ln d \propto \ln N$, leads to somewhat smaller tails than in a Θ solvent. However, in both cases tails may become rather long in not too dilute solutions.

2.5. Train, Loop, and Tail Size Distribution. In the previous section we derived the train size distribution starting from the discrete lattice equations. The result may be written as

$$n^{tr}(s) = A^{tr}(N - s)e^{-\epsilon s}(\lambda_0 G_1)^s, \quad A^{tr} = \frac{\lambda^2 {g_2}^2}{\lambda_0 \Gamma} \qquad (24a,b)$$

This result contains only the field u_1 in the surface layer ($G_1 = e^{-u_1}$) since all the train segments experience the same field u_1, which through the boundary condition I-28 is related to the ratio g_1/g_2. For $s << N$ eq 24a may be rewritten as $n^{tr}(s) \propto r^s$, where $r = \lambda_0 G_1 e^{-\epsilon - 1/N}$. As in the previous section $l^{tr} = (1 - r)^{-1}$, which gives a slightly more accurate expression for l^{tr} than that in eq 20b (the difference is just the factor $e^{-1/N}$ in r). Hence, $n^{tr}(s)$ can be written in terms of l^{tr} only. If we define the fraction of trains of length s through $f^{tr}(s) = n^{tr}(s)/n^{tr}$, we find

$$f^{tr}(s) = \frac{1}{l^{tr}}\left(1 - \frac{1}{l^{tr}}\right)^{s-1} \qquad (25)$$

which is identical to an expression derived in early work by Hoeve et al.[8,9] Apparently, trains of size 1 are the most abundant, with $f^{tr}(1) = 1/l^{tr}$. It has been shown[4] that eq 25 reproduces the numerical train size distribution very accurately, provided the numerical result for l^{tr} is used as the input in this equation. In other words, eq 25 nearly exactly predicts the spread of the train sizes around the average.

For loops the discretized size distribution is given by eq 17a. Using again the GSA result $G = b^{-1}ge^{\epsilon s}$ and $\varphi^b e^{\epsilon N} = b^2$, we find for the continuum analogue

$$n^l(s) = A^l(N - s)W^l(s), \quad W^l(s) = e^{-\epsilon s}G^t_{2,s}, \quad A^l = \frac{\lambda^2 {g_1}^2}{\Gamma} \qquad (26a,b,c)$$

We neglected 1 with respect to $N - s$ and introduced the function $W^l(s)$ as defined in eq 26b. This function can be found by solving the appropriate differential equation (which is the analogue of the discrete propagator relation in the numerical model), using the boundary conditions for free walks that start and end in layer 2. Details are given in Appendix I. The solution is found using Laplace transforms and, in its full form, is a rather lengthy equation (eq AI-7). Here we give only the simplified expression for long chains, obtained by expansion of the solution in terms of $1/d$ to lowest order. For a good solvent the (unnormalized) result is

$$G^t_{2,s} = W^l(s)e^{\epsilon s} \propto \left(\frac{{p_3}^2}{\sqrt{\lambda s}} - 2\sqrt{\lambda s}\right)(1 - e^{-1/4\lambda s}) + \frac{\sqrt{\pi}}{2p_2}e^{1/p_2 + \lambda s/p_2^2}\,\mathrm{erfc}\left(\frac{\sqrt{\lambda s}}{p_2} + \frac{1}{2\sqrt{\lambda s}}\right) \qquad (27)$$

where $\mathrm{erfc}\, x = 1 - \mathrm{erf}\, x$ is the complementary error function. The normalization factor can be chosen such that $G^t_{2,1}$ becomes equal to $G_2 = e^{-u_2}$, which is the starting condition for the recurrence relation for $G^t_{z,s}$ in the lattice model. Unfortunately, even this limiting expression for long chains looks rather complicated. For $s >> 1$, it may be expanded in terms of $1/\lambda s$ to lowest order, which gives $G^t_{2,s} \propto s^{-5/2}$. This power law is the same as derived for the loop size distribution $n^l(s)$ in a mean-field variant of the scaling approach as given by Bouchaud and Daoud[10] and De Gennes.[11] This scaling picture, which gives $n^l(s) \propto s^{-5/2}$ in a (mean-field) good solvent, is summarized in Appendix II. We note that the exponent $-{}^5/_2$ for loops in the field $u(z)$ is markedly different from the random-walk (zero field) result $-{}^3/_2$ obtained by Hoeve.[8,9]

In principle, a similar result could be obtained for the loop size distribution in a Θ solvent. The equations are even more complex, and we do not pursue this point. The scaling treatment can be done without extra effort (Appendix II). The result is $n^l(s) \propto s^{-2}$ for a Θ solvent. The exponent is thus closer to Hoeve's random-walk result, which is not surprising because the field in a Θ solvent is smaller than in a good solvent.

For the tail size distribution in the continuum version we express $G^f_{2,s}$ in eq 18a as a sum of $G^t_{z,s}$ over all layers $z > 1$: unlike loops, which have to return to a specific layer ($z = 2$, so that for loops we need only $G^t_{2,s}$), tails may end up anywhere. We now introduce a function $W^t(z,s) = e^{-\epsilon s}G^t_{z,s}$, which is a generalization of $W^l(s)$ in eq 26: $W^l(s)$ equals $W^t(2,s)$. Hence,

$$n^t(s) = A^t\sum_z W^t(z,s), \quad W^t(z,s) = e^{-\epsilon s}G^t_{z,s}, \quad A^t = \frac{2b\lambda g_2}{\Gamma} \qquad (28a,b,c)$$

An expression for $W^t(z,s)$ is derived in in Appendix I (eq AI-7). As expected, the result is even more complex than that for $W^l(s)$. Although $W^t(z,s)$ could be expanded in terms of $1/d$ to give a similar (though even lengthier)

expression as the one in eq 27, this does not help in finding a "simple" equation for $n^t(s)$ because of the sum (integration) in eq 28a. Hence, eq AI-7 is our only analytical result for the tail size distribution. A scaling description for the tail size distribution gives the power law $n^t(s) \propto s^{-1}$ in a good solvent (Appendix II). A random-walk model results in an exponent $-1/2$.[8,9]

As for loops, we do not attempt to derive the full tail size distribution for a Θ solvent, and we restrict ourselves to mentioning the scaling result as derived in Appendix II: $n^t(s) \propto s^{-3/4}$ for a Θ solvent. As expected, this exponent is closer to the random-walk exponent $-1/2$ than in a good solvent, where the field is higher.

3. Results

In this section, we compare in some detail the predictions of the analytical model with the full numerical data, for both a good solvent ($\chi = 0$) and a Θ solvent ($\chi = 0.5$). We consider the adsorbed amounts in trains, loops, ands tails (Figures 2−4), structural details of the adsorbed layer (Figures 5−10), and the number and average length of trains, loops, and tails (Figures 11−15). Finally, we give an example of train, loop, and tail size distributions (Figures 16−18). We choose a hexagonal lattice ($\lambda = 1/4$) because for this lattice type relatively many numerical results have been published.[3−5]

In all the figures, we present the numerical data as solid ($\chi = 0$) or dashed ($\chi = 0.5$) curves and the simplest analytical approximation (i.e., the uncoupled solution for the plateau region, with the proximal length p calculated from eq 1 and the distal length d from eq 7) as symbols. For this solution, the full hyperbolic functions were used (hence, for example sinh x was not replaced by x); we refer to this solution as the "plateau approximation". All the results were also calculated with the more accurate approximation where p and d are obtained from the coupled eqs I-27 and 28 ("coupled approximation"). Since in most cases this solution is nearly the same as the plateau approximation, the coupled approximation is then not given in the figures. Only in some situations when there is a difference (e.g., for results in the Henry regime) is the coupled approximation shown separately; in those cases this solution is given as dotted curves.

3.1. Adsorbed Amounts in Trains, Loops, and Tails. Figure 2 shows Γ^{tr} as a function of the adsorption energy χ_s (Figure 2a) and as a function of the chain length N (Figure 2b). For long chains, Γ^{tr} depends only on χ_s (eq 8), and it is inversely proportional to p_1^2 for $\chi = 0$ and to p_1 for $\chi = 0.5$; the way in which the parameter p_1 varies with χ_s is plotted in Figure I-6 (in fact, this figure gives $\sqrt{\Gamma^{tr}}$). It is clear from Figure 2a that the plateau approximation works quite well over the entire range of χ_s. The curve for $\chi = 0$ is sigmoidal due to the p_1^2 dependence. The surface is half-occupied for a value of χ_s corresponding to $p_1^2 = 2q^2$ ($\chi = 0$) or $p_1 = 2q$ ($\chi = 0.5$), where $q = p_\infty - 1/2$ is defined in eq 1; this equation gives $\chi_s = 1.16$ and $\chi_s = 0.627$, respectively, for these midpoints. Above these values of χ_s the surface saturates, with Γ^{tr} approaching unity exponentially: $\Gamma^{tr} \approx 1 - Ae^{-\chi_s}$, as is easily derived from the $p_1(\chi_s)$ dependence for high χ_s (eqs I-45c and 47c). The prefactor A depends only on the lattice type and with $\lambda = 1/4$ equals $A = 1.66$ for $\chi = 0$ and $A = 0.744$ for $\chi = 0.5$; these asymptotic exponential dependencies are also plotted in Figure 2a.

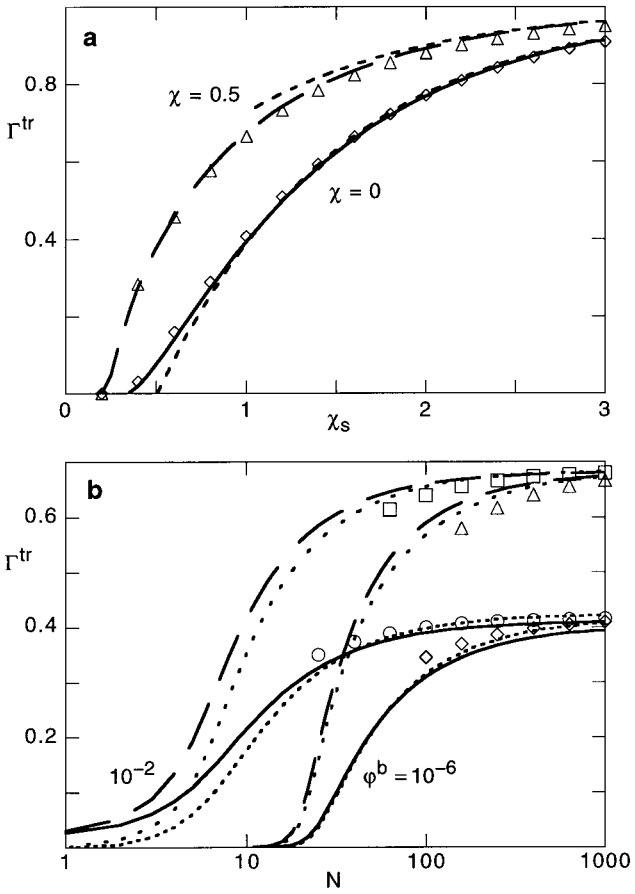

Figure 2. Adsorbed amount Γ^{tr} in trains as a function of χ_s (for $N = 10^3$ and $\varphi^b = 10^{-6}$) (a) and as a function of the chain length N (for $\chi_s = 1$ and $\varphi^b = 10^{-6}$ and 10^{-2}) (b). The solid and dashed curves are numerical results for $\chi = 0$ and $\chi = 0.5$, respectively. Symbols represent the plateau approximation: they are given only for $x_1 < 1$. In (a) the short dashes represent the high χ_s approximations $\Gamma^{tr} = 1 - Ae^{-\chi_s}$, with $A = 1.66$ for $\chi = 0$ and $A = 0.744$ for $\chi = 0.5$. In (b) the dotted curves are the coupled approximation.

For long enough chains, Γ^{tr} is independent of N and φ^b, as seen in Figure 2b; the $(p_1/d)^2$ correction in eqs 8g and 8t is then negligible. For smaller N (down to values around 100) this correction does play a role, and the ratio between Γ^{tr} and its long-chain limit Γ^{tr}_∞ can be written as $1 - AY^2/N$, where the numerical factor A equals $(4/3)p_1^2 \approx 1.6$ for $\chi = 0$ and $(8/3)p_1^2 \approx 2.2$ for $\chi = 0.5$. When this correction term becomes appreciable, the plateau approximation (in which p_1 is calculated assuming $\sinh x_2/\sinh x_1 = x_2/x_1$) breaks down; in Figure 2b the symbols for this approximation are only given for $x_1 < 1$. The coupled analytical approximation works quite well, even for rather small N, when the surface is undersaturated and the equations for the Henry region apply.

A similar set of plots for the adsorbed amount Γ^l in loops is given in Figure 3. The agreement between the analytical and the numerical model is rather good, but it is less accurate than for Γ^{tr} (Figure 2). The analytical model underestimates the loop contribution systematically by 10−20%. The reason for this deviation was discussed extensively in part I; the main point is that the eigenfunction g_z is underestimated in several layers adjoining the train layer. Allowing for these systematic differences, we see that the trends for Γ^l are nevertheless well described by the analytical model.

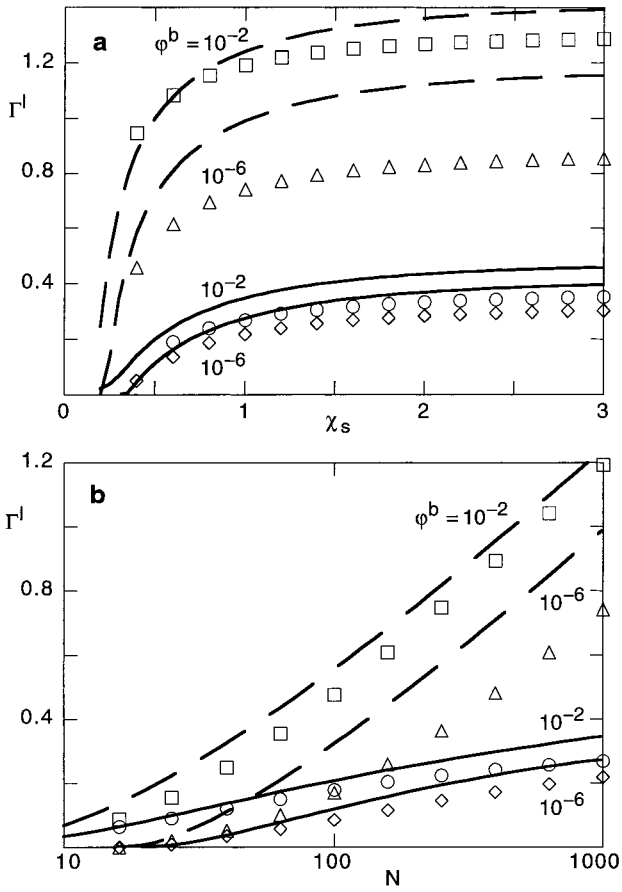

Figure 3. Adsorbed amount Γ^l in loops as a function of χ_s (for $N = 10^3$ and $\varphi^b = 10^{-6}$ and 10^{-2}) (a) and as a function of the chain length N (for $\chi_s = 1$ and $\varphi^b = 10^{-2}$ and 10^{-6}) (b). The solid and dashed curves are numerical results for $\chi = 0$ and $\chi = 0.5$, respectively. Symbols represent the plateau approximation.

For high χ_s and in the good solvent, Γ^l in the analytical model reaches for long chains a limiting value $\Gamma^l_\infty \approx q^2/(p_\infty + 1) \approx 0.4$, where the $1/d$ correction in eq 8g is negligible. In Figure 3a this is not yet the case for the "analytical" data (symbols). In a Θ solvent, the high χ_s limit is higher (and a function of N, see Figure 3b), but the general shape $\Gamma^l(\chi_s)$ is the same. Just as for Γ^{tr}, the approach toward this limit is exponential in χ_s: $\Gamma^l = \Gamma^l_\infty - Ae^{-\chi_s}$, where $A = 0.29$ for $\chi = 0$ and $A = 0.56$ for $\chi = 0.5$.

Figure 3b shows the chain-length dependence of Γ^l. For $\chi = 0$ a limit at high N is reached (0.4 as discussed above), but in a Θ solvent Γ^l increases logarithmically with N; the slope $d\Gamma/d \log N$ equals $2.3q/2 \approx 0.7$, so that Γ^l increases by 0.7 monolayers for every decade in N. This linear increase with log N persists up to much higher chain lengths than indicated in Figure 3b.[5]

The concentration dependence of Γ^l is very weak. In a good solvent, it is absent for very long chains (where the p_2/d correction in eq 9g vanishes). In Figure 3b the chains are still too short to reach this limit, though it can be seen that the analytical curves for the two concentrations tend to converge. In a Θ solvent there is a weak effect due to the term ln d in eq 9t; the concentration-dependent part in this term is $\ln y = {}^1/_2 \ln(\ln(1/\varphi^b))$. The curves $\Gamma^l(N)$ for different φ^b run parallel, with a constant difference. For example, the difference $(q/2)(\ln \ln 10^6 - \ln \ln 10^2)$ between $\varphi^b = 10^{-2}$ and 10^{-6} in Figure 3b would be about 0.34 if Y is replaced by y (i.e., if the ln b correction in eq 7b is neglected). For $\varphi^b = 10^{-2}$ this correction is appreciable, and the difference $(q/2)(\ln Y_1 - \ln Y_2)$ is higher, in this case 0.48. This does indeed correspond to the difference between the squares and the triangles in Figure 3.

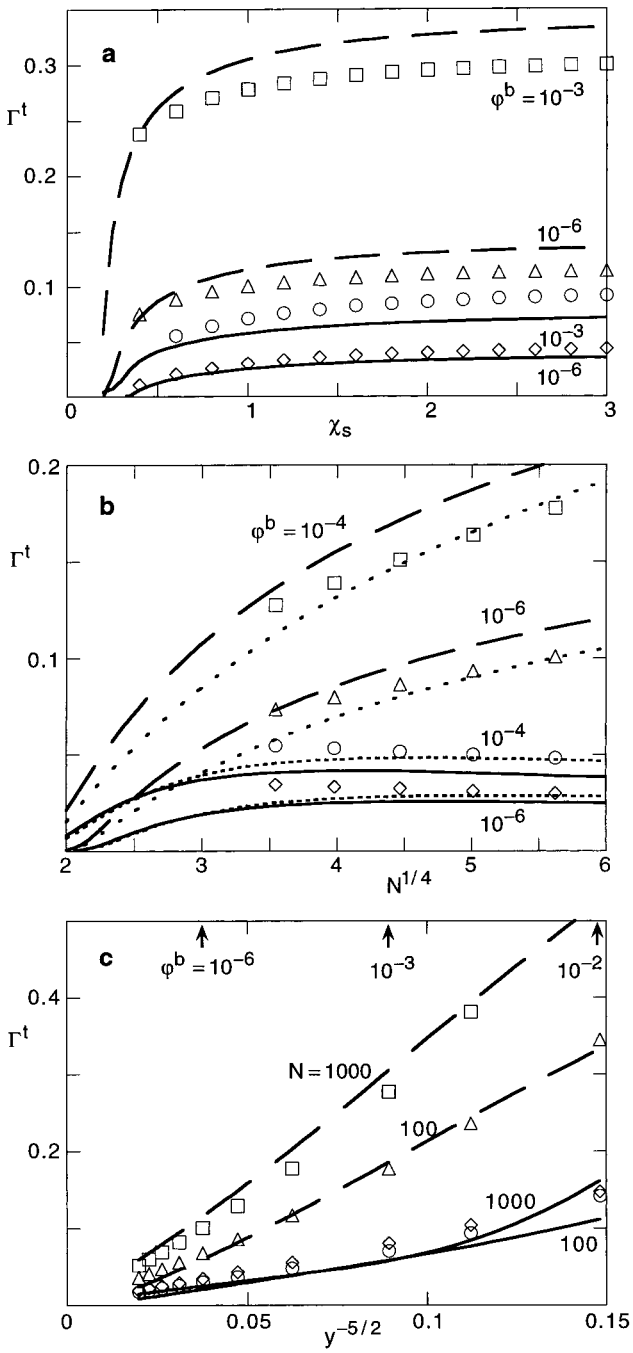

Figure 4. Adsorbed amount Γ^t in tails as a function of χ_s (for $N = 10^3$ and $\varphi^b = 10^{-6}$ and 10^{-3}) (a), as a function of $N^{1/4}$ (for $\chi_s = 1$ and $\varphi^b = 10^{-6}$ and 10^{-4}) (b), and as a function of $y^{-5/2}$ (for $\chi_s = 1$ and $N = 10^2$ and 10^3) (c). The solid and dashed curves are numerical results for $\chi = 0$ and $\chi = 0.5$, respectively. Symbols are the plateau approximation (given only for $x_1 < 1$). The dotted curves in (b) represent the coupled approximation.

Figure 4 gives the adsorbed amount Γ^t in tails as a function of the adsorption energy (Figure 4a), the chain length (Figure 4b), and the bulk concentration (Figure 4c). According to eq 10, the χ_s dependence shows up mainly in the factor $\sqrt{\Gamma^{tr}}$, so that in Figure 4a the increase of Γ^t with χ_s is weaker than that of Γ^{tr} (Figure

2a); for not too low χ_s it may be described as $\Gamma^t/\Gamma^t_\infty = 1 - Ae^{-\chi_s}$, where the prefactor is half that for Γ^{tr}: $A = 0.83$ for $\chi = 0$ and $A = 0.372$ for $\chi = 0.5$. The concentration dependence is rather strong: Y^{-2} for $\chi = 0$ and $Y^{-5/2}$ for $\chi = 0.5$. For $\varphi^b = 10^{-3}$ and 10^{-6}, this gives in Figure 4a a ratio of about 2 for $\chi = 0$ and of $2^{5/4} = 2.38$ for $\chi = 0.5$. At given φ^b, Γ^t is higher in a Θ solvent by a factor $0.92N^{1/4}Y^{-1/2}$. With $N = 10^3$ this ratio in Figure 4a is 2.64 for $\varphi^b = 10^{-6}$ and 3.21 for $\varphi^b = 10^{-3}$.

Figure 4b gives more detail about the chain-length dependence of Γ^t. In a good solvent $\Gamma^t \propto \alpha\sqrt{\Gamma^{tr}}$ according to eq 10g. For $N > 100$, Γ^{tr} is roughly constant (Figure 2b) and there is only a weak effect due to the factor $\alpha \approx 1 - 0.15 \log N$ (see Figure 1), so that Γ^t decreases very weakly with increasing N. This effect shows up both in the numerical data and the analytical approximations; the symbols representing the plateau approximation in Figure 4b are again given only for $x_1 < 1$. For smaller N, Γ^{tr} decreases relatively strongly (Figure 2b), so that Γ^t passes through a maximum. The plateau approximation breaks down for those short chains; however, the coupled analytical solution (dotted curve) works quite well, even for rather small N.

In a Θ solvent the factor $N^{1/4}$ in eq 10t causes Γ^t to increase with N, so that there is no maximum. At high N the increase is approximately linear in $N^{1/4}$ (although the logarithmic decrease of α with N produces a slight downward curvature). For shorter chains the dependence $\Gamma^t(N)$ becomes stronger because now also Γ^{tr} decreases. It is gratifying to note that the analytical approximations, though underestimating Γ^t slightly for $\chi = 0.5$, reproduce the trends of the full numerical model neatly.

Figure 4c shows, for $N = 100$ and 1000, the concentration dependence of Γ^t explicitly. In this figure Γ^t is plotted against $y^{-5/2}$, which according to eq 10t should give a straight line for $\chi = 0.5$, with a slope which is a factor $10^{1/4} = 1.78$ higher for $N = 1000$. This is approximately the case, although the analytical model shows some deviations for $N = 1000$ and concentrations above 10^{-3}; in this range the difference between Y and y (eq 6b) is relatively more important. Moreover, the present analytical model is not adequate for long chains in concentrated solutions. Although $N = 1000$ and $\varphi^b = 10^{-3}$ is still in the dilute regime, corrections are to be expected. For $\chi = 0$ the adsorbance is dominated by small loops and trains up to fairly high concentrations. These contribute about one monolayer to the adsorbance, and the contribution of large loops extending up to the radius of gyration is of order of $\varphi^b N^{1/2}$, which dominates only for $\varphi^b \geq N^{-1/2}$, where the ground-state dominance for loops fails. This concentration is well above the overlap concentration $\propto 1/N$. For the Θ solvent the two characteristic concentrations are both of order $N^{-1/2}$, and corrections become important already in the dilute regime.

For $\chi = 0$ a straight line would be found in Figure 4c if Γ^t would be plotted against y^{-2}. In a plot as a function of $y^{-5/2}$ an upward curvature shows up. As expected, the chain-length dependence in this case is nearly absent: the two curves for $N = 100$ and 1000 in Figure 4c nearly coincide (except for very high φ^b).

3.2. Structural Aspects. In section 2.3 we presented the equations for the distances z_l and z_t where the concentration of loops and tails, respectively, become equal to φ^b, for the position (z_m) and height (φ_m) of the maximum in the tail profile, and for the cross-over distance z^* between loops and tails. In this section, we compare these predictions with the numerical SCF results.

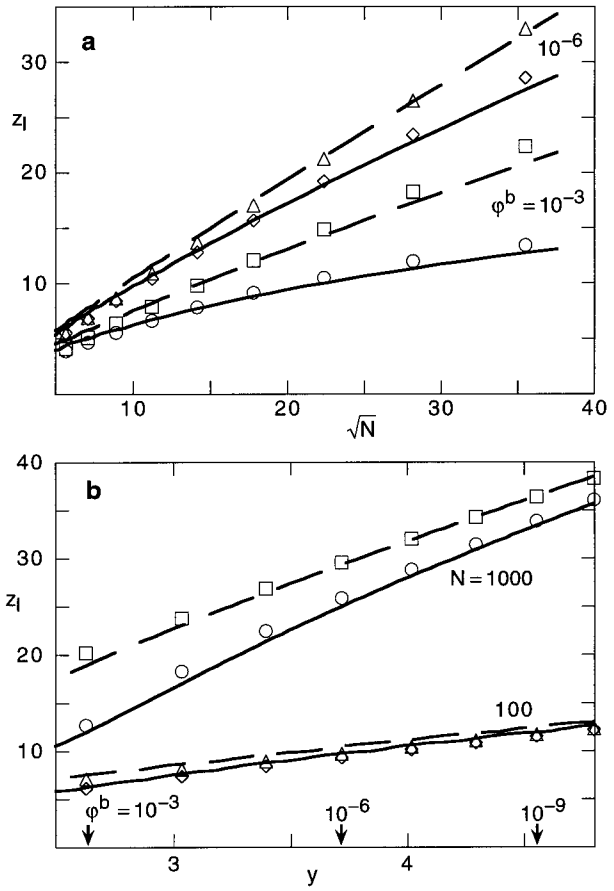

Figure 5. Distance z_l at which the loop concentration becomes equal to φ^b as a function of $N^{1/2}$ (for $\chi_s = 1$ and $\varphi^b = 10^{-6}$ and 10^{-3}) (a), and as a function of y (for $\chi_s = 1$ and $N = 10^2$ and 10^3) (b). The solid and dashed curves are numerical results for $\chi = 0$ and $\chi = 0.5$, respectively. Symbols give the plateau approximation.

Figure 5 gives z_l as a function of $\sqrt{N}$ (Figure 5a) and as a function of $y = \sqrt{\ln(1/\varphi^b)}$ (Figure 5b). According to eq 11, $z_l \propto dx_l$ is expected to vary approximately as $^1/_2 d(y^2 - 2 \ln d)$ for $\chi = 0$ and as $^1/_2 d(y^2 - \ln d)$ for $\chi = 0.5$. Since $d \approx {}^1/_2\sqrt{N}/y$, these dependencies can be written as $^1/_4\sqrt{N}(y - 2y^{-1} \ln d)$ and $^1/_4\sqrt{N}(y - y^{-1} \ln d)$, respectively. Figure 5a confirms the approximate $\sqrt{N}$ dependence and Figure 5b the y dependence. In both figures the linearity is more accurately obeyed for $\chi = 0.5$ (where the ln d correction is smaller by a factor of 2). The agreement between the analytical model and the numerical data is very good in these figures.

A similar comparison is made for z_t in Figure 6. In this case the approximate dependence is $z_t \approx d(y^2 - \ln d)$ for $\chi = 0$, and $z_t \approx d(y^2 - {}^1/_2 \ln d)$ for $\chi = 0.5$, about twice z_l. Apart from this factor of 2, the trends for z_t as a function of $\sqrt{N}$ (Figure 6a) and as a function of y (Figure 6b) are quite comparable with those for z_l (Figure 5).

Figure 7 shows how the position z_m of the tail maximum depends on the chain length (Figure 7a) and on the concentration (Figure 7b). The parameter z_m is, according to eq 13, essentially only determined by the distal length d; the analytical curves in Figure 7 may

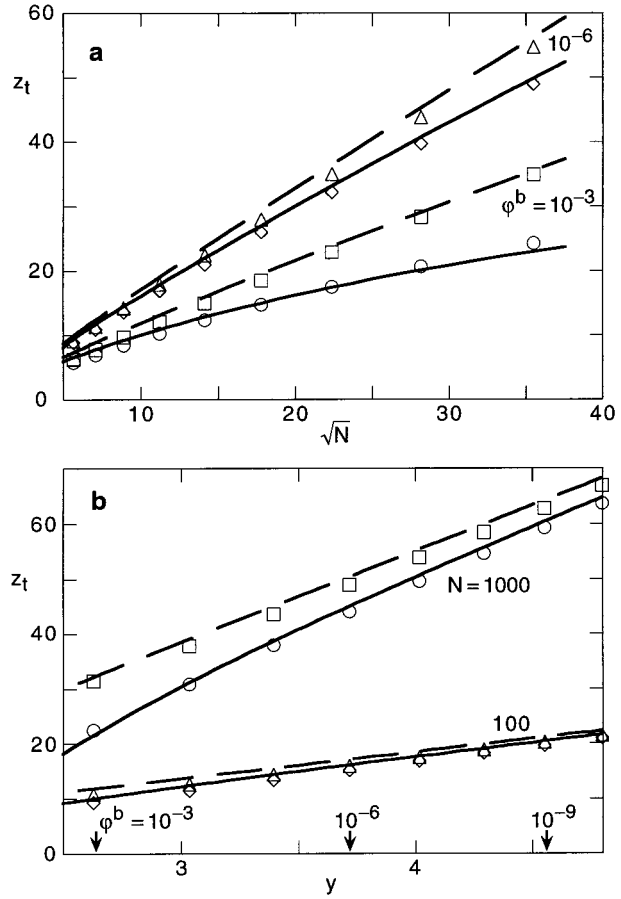

Figure 6. As Figure 5, but now for the distance z_t where the tail concentration becomes equal to the bulk concentration.

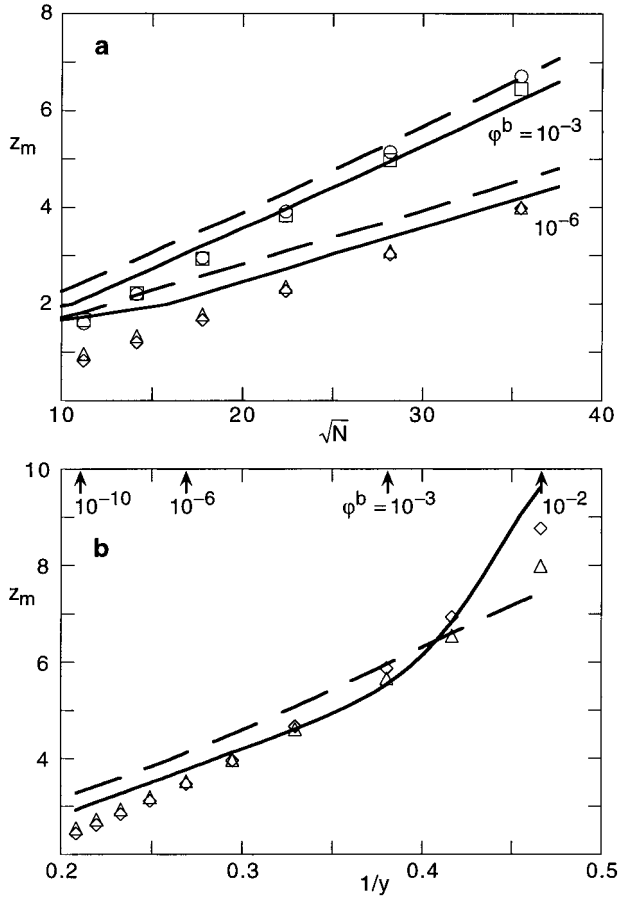

Figure 7. Distance z_m corresponding to the maximum in the tail segment profile as a function of $N^{1/2}$, for $\chi_s = 1$ and $\varphi^b = 10^{-6}$ and 10^{-3} (a), and as a function of $1/y$ (for $\chi_s = 1$ and $N = 10^3$) (b). The solid and dashed curves are numerical results for $\chi = 0$ and $\chi = 0.5$, respectively. Symbols represent the plateau approximation.

thus also be seen as plots $d(\sqrt{N})$ or $d(1/y)$. Accordingly, $z_m \propto \sqrt{N}/y$, so that z_m becomes higher in more concentrated solutions (unlike z_l and z_t, which decrease since they are directly proportional to y). In Figure 7b we give only data for $N = 1000$, since for short chains (e.g., $N = 100$) the tail maximum is situated in the second layer. The agreement in Figure 7 between analytical and numerical results is fair, but less perfect than for z_l and z_t (Figures 5 and 6). The reason is clear: in the analytical model the approximation was made to replace $\epsilon + u$ by $\epsilon + \varphi^1$ or by $\epsilon + (\varphi^1)^2/2$ (see eq I-17), which is relatively inaccurate around the tail maximum. Nevertheless, even in this region the analytical model predicts the trends quite satisfactory.

In Figure 8 the height of the tail maximum is plotted as a function of χ_s (Figure 8a), as a function of $N^{-1/2}$ (Figure 8b), and as a function of $1/y$ (Figure 8c). According to eq 14, the χ_s dependence is determined mainly by the factor $\sqrt{\Gamma^{tr}}$, so that Figure 8a for φ_m closely resembles Figure 4a for Γ^t. The only difference is the weaker concentration dependence of φ_m ($\propto Y^{-1}$ for $\chi = 0$, $\propto Y^{-3/2}$ for $\chi = 0.5$) as compared to Γ^t (where $\Gamma^t \propto Y^{-2}$ and $Y^{-5/2}$, respectively).

Figure 8b shows the chain-length dependence of φ_m over the range $N > 100$. For shorter chains the data are less relevant because, as discussed above (Figure 7), for $N < 100$ the tail maximum is always in the second layer. Equation 14g predicts that φ_m should be linear in $N^{-1/2}$ as long as Γ^{tr} is constant; the proportionality factor should be inversely proportional to Y. These features are indeed found in Figure 8b. For $\chi = 0.5$, $\varphi_m \propto N^{-1/4}$ so that a plot $\varphi_m(N^{-1/2})$ is curved; moreover, φ_m is higher than in a good solvent (the ratio between the two is $N^{1/4}/Y^{1/2}$).

Figure 8c gives an explicit check on the concentration dependence of φ_m. The plot $\varphi_m(y^{-1})$ is nearly straight for a good solvent, as expected on the basis of eq 14g; the ratio between the slopes for the two chain lengths shown is $10^{1/2} = 3.2$. For a Θ solvent, the concentration dependence is stronger ($Y^{-3/2}$) so that in Figure 8c the curves bend upward; the effect of the chain length is weaker, with a factor $10^{1/4}$ between the two chain lengths.

We conclude this section with the chain-length and concentration dependence of the crossover distance z^*. Analytical equations for situations where $z^* > d$ were given in eq 15. We plot both z^* (Figure 9) and the ratio z^*/d (Figure 10). Figure 9a shows that z^* is larger than d for $\chi_s = 1$ and $\varphi^b = 10^{-6}$ and that both z^* and d increase roughly proportionally to $\sqrt{N}$ in the range $N = 100-1500$, as expected from eq 15. The analytical results for z^* are about 10% higher than the numerical ones but show the same trends. The ratio z^*/d (Figure 10a) decreases gradually with increasing chain length. This decrease is stronger in a good solvent than in a Θ solvent, on account of the $1/d$ term in the logarithmic factor of eq 15g, as compared to $1/\sqrt{d}$ in eq 15t. A rough extrapolation of the numerical data suggests that z^*/d becomes unity around $N = 5 \times 10^4$, which would then indicate the upper limit of our present analytical

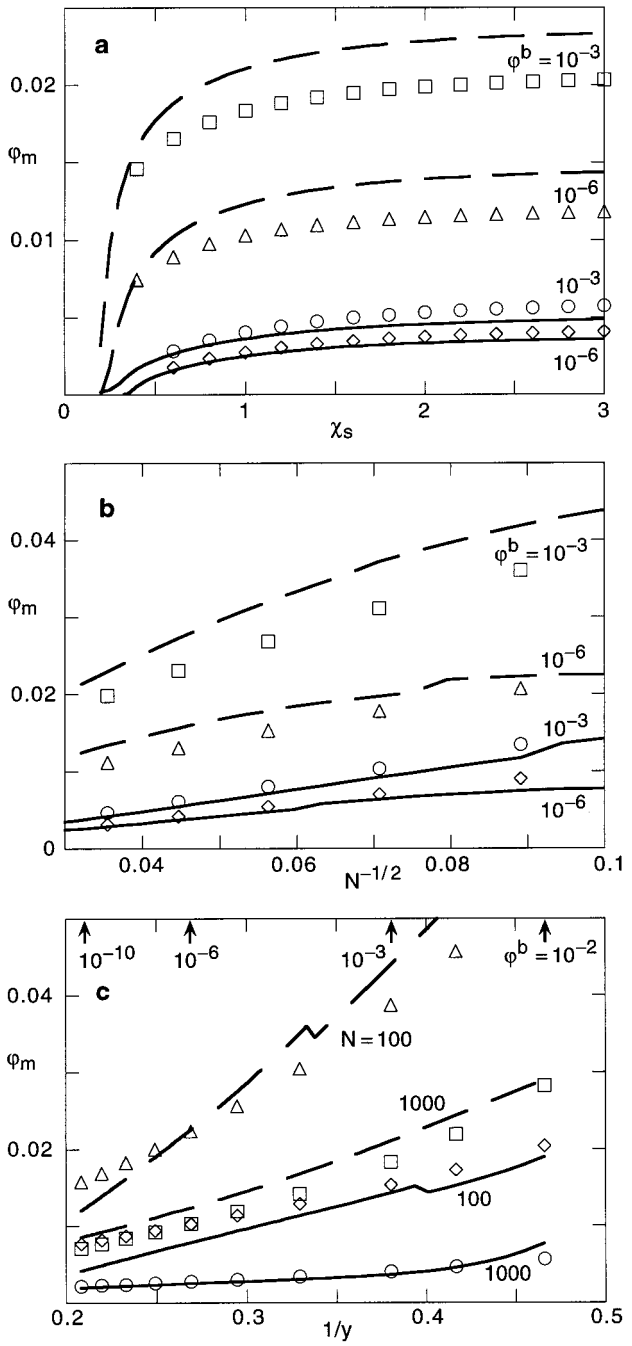

Figure 8. Height φ_m of the maximum in the tail segment profile as a function of χ_s (for $N = 10^3$ and $\varphi^b = 10^{-6}$ and 10^{-3}) (a), as a function of $N^{-1/2}$ (for $\chi_s = 1$ and $\varphi^b = 10^{-6}$ and 10^{-3}) (b), and as a function of y^{-1} (for $\chi_s = 1$ and $N = 10^2$ and 10^3) (c). The solid and dashed curves are numerical results for $\chi = 0$ and $\chi = 0.5$, respectively; the irregularities represent inaccuracies in the interpolation procedure to find φ_m from values of φ^t in three layers around the maximum. Symbols are the plateau approximation.

model for a good solvent (cf. the discussion above eq 15). Published data[6] for z^* for very long chains and $\lambda = {}^1/_6$ give the same order of magnitude for the chain length where z^*/d becomes unity. For a Θ solvent this upper limit is much higher and the validity range correspondingly wider.

The original theory by Semenov et al.[2] predicted that z^* should scale as $N^{1/3}$. From our present analytical model (eq 15) there is no direct justification for this exponent: eq 15 predicts z^* to be proportional to $d \propto \sqrt{N}$ with, however, a logarithmic correction which

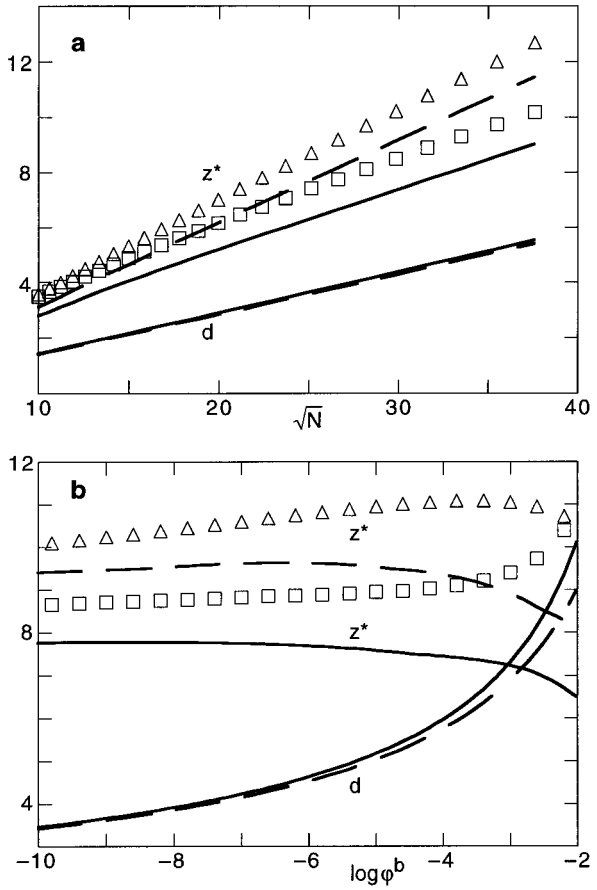

Figure 9. Crossover distance z^* and the distal length as a function of $\sqrt{N}$ for $\chi_s = 1$ and $\varphi^b = 10^{-6}$ (a) and as a function of log φ^b ($=-0.43y^2$) for $\chi_s = 1$ and $N = 10^3$ (b). Solid curves represent the distal length and numerical results for z^* in a good solvent and dashed curves refer to a Θ solvent. Symbols are the plateau approximation for z^*.

makes the dependence weaker than $N^{1/2}$. This is due to the fact that we constructed our theory on the basis of the distal length d rather than on z^*, which is reasonable for "normal" chain lengths. Plotting $z^*(N)$ on a double-logarithmic scale gives, in the range $500 < N < 1500$, nevertheless a more or less straight line with a slope 0.37. An exponent very close to ${}^1/_3$ was found by Johner et al.[6] for much longer chains ($5.10^3 < N < 10^5$). In most of the latter range the length z^* is indeed relevant (being then smaller than d), so that an exponent ${}^1/_3$ should apply (apart from some logarithmic corrections). Obviously, a precise scaling behavior can only be expected far from the crossover $z^* = d$. As shown before,[6] numerical integration of the partial differential equations gives good results. We conclude that the theory by Semenov et al.[2] corresponds to the limit $z^* << d$, whereas in the present paper (and in part of ref 6) the opposite case $z^* > d$ is considered.

The concentration dependence of z^* and z^*/d is illustrated in Figures 9b and 10b. In Figure 9b also the distal length is plotted. As this parameter is approximately inversely proportional to $y = \sqrt{\ln(1/\varphi^b)}$, which varies from 4.8 at $\varphi^b = 10^{-10}$ to 2.6 at $\varphi^b = 10^{-3}$ (and 2.1 at $\varphi^b = 10^{-2}$, where our approximation breaks down), d increases in the same (inverse) ratio. Nevertheless, z^* is nearly independent of φ^b (Figure 9b), in both the analytical and numerical descriptions. If the constant in the logarithmic terms of eq 15 is neglected, z^* is approximately proportional to y^{-1} ln y, which

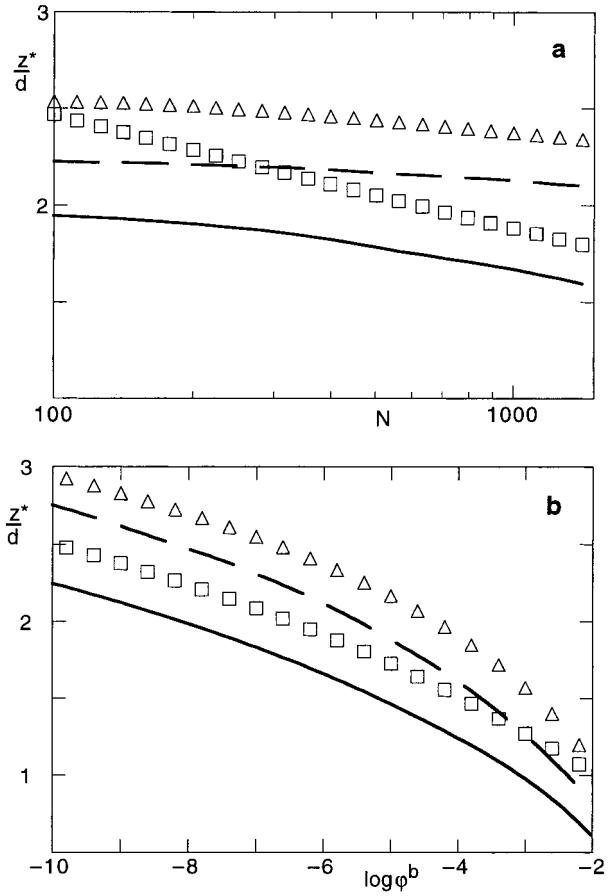

Figure 10. Ratio z^*/d as a function of N for $\chi_s = 1$ and $\varphi^b = 10^{-6}$ (a) and as a function of log φ^b ($= -0.43y^2$) for $\chi_s = 1$ and $N = 10^3$ (b). Solid curves represent the numerical results for a good solvent, and dashed curves refer to a Θ solvent. Symbols are the plateau approximation.

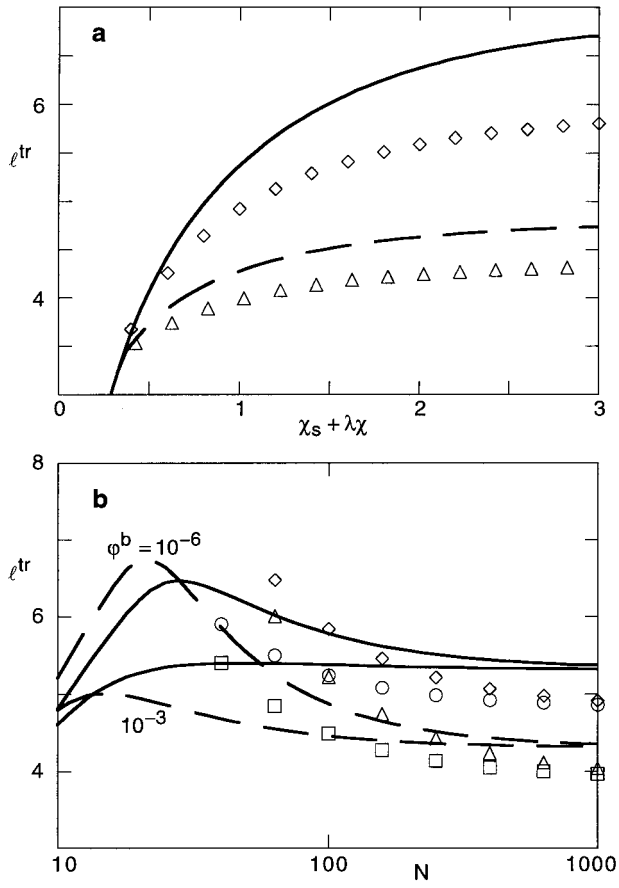

Figure 11. Average length of the trains as a function of $\chi_s + \lambda\chi$ (for $N = 10^3$ and $\varphi^b = 10^{-6}$ and 10^{-3}) (a) and as a function of N (for $\chi_s = 1$ and $\varphi^b = 10^{-6}$ and 10^{-3}) (b). The solid and dashed curves are numerical results for $\chi = 0$ and $\chi = 0.5$, respectively. Symbols represent the plateau approximation.

function over the given range of y does indeed depend only very weakly on y. Since z^* is nearly independent of φ^b in the range $10^{-10}-10^{-2}$, the ratio z^*/d decreases with increasing concentration (Figure 10b) because d increases (Figure 9b). In the numerical data, this ratio becomes unity around $\varphi^b = 10^{-3}$ in a good solvent and around $\varphi^b = 5 \times 10^{-3}$ in a Θ solvent. At these relatively high concentrations the analytical model breaks down, as is also to be expected from other considerations (e.g., because of free state contributions at concentrations in the dilute regime approaching the overlap concentration). The deviations between the analytical and numerical data become therefore also stronger in such concentrated solutions. For much longer chains ($N = 4 \times 10^4$) the concentration at which z^*/d becomes unity is lower (around 10^{-4} for $\chi = 0$),[6] which is the expected result.

3.3. Number and Length of Trains, Loops, and Tails. Analytical approximations for the length of trains, loops, and tails and for the number of these sequences per adsorbed chain were given in eqs 20−23. Figures 11−15 provide a comparison between these predictions and the numerical results.

Figure 11 displays the train length l^{tr} as a function of χ_s (Figure 11a) and N (Figure 11b). According to eq 19b, l^{tr} for long chains is only a function of χ_s, since the ratio g_1/g_2 equals p_3/p_1 ($\chi = 0$) or $\sqrt{p_3/p_1}$ ($\chi = 0.5$). At $\chi_s = \chi_{sc}$, where $1/p_1 = 0$, g_1/g_2 approaches unity. (This remains valid if the equations for the Henry region are used, because $g_1/g_2 = e^{1/d_h}$ becomes unity as d_h diverges). Hence, l^{tr} reaches the lower limit $1 + \lambda_0/\lambda$ at critical adsorption. In order to make a fair comparison, in Figure 11 (and the following figures) we do not use χ_s as the variable, but $\chi_s + \lambda\chi$. In this way the critical point is reached at the same value of $\chi_s + \lambda\chi$. As χ_s increases, l^{tr} increases as well, but it levels off when p_1 approaches its limiting value q. This approach is again exponential. For example, for $\chi = 0$ we have $l^{tr}_\infty - l^{tr} = (\lambda_0/\lambda)(1/q - 1/p_1) = Ae^{-\chi_s}$, where A equals $1.66\sqrt{2} = 2.35$. The general trends for $l^{tr}(\chi_s)$ are the same in the analytical and numerical models, but the analytical equations underestimate l^{tr} by about 20% (i.e., by about one segment for high χ_s).

The chain-length dependence of l^{tr} is shown in Figure 11b. For long chains there is no effect of N. As the chains become shorter, l^{tr} increases because $\sinh x_3/\sinh x_1$ increases more strongly than x_3/x_1 (which is only a function of χ_s). Using again $\sinh x = x + x^3/6$, we derive easily that the increase is by a factor $1 + AY^2/N$, where $A = 4/3p_1$ for $\chi = 0$ and $8/3p_1$ for $\chi = 0.5$. Hence, this increase is stronger in a Θ solvent. For still smaller N the numerical data for $l^{tr}(N)$ pass through a maximum (obviously, very short chains cannot develop trains of length 5). This maximum is not predicted analytically. One reason is the fact that, for convenience, we replaced the factor $N - s$ in eq 24a by N, which could have been avoided. However, the analytical model breaks down anyhow for very low N.

Figure 12 gives similar information on the loop length. The trends in Figure 12a, which gives $l^{tr}(\chi_s)$, are most

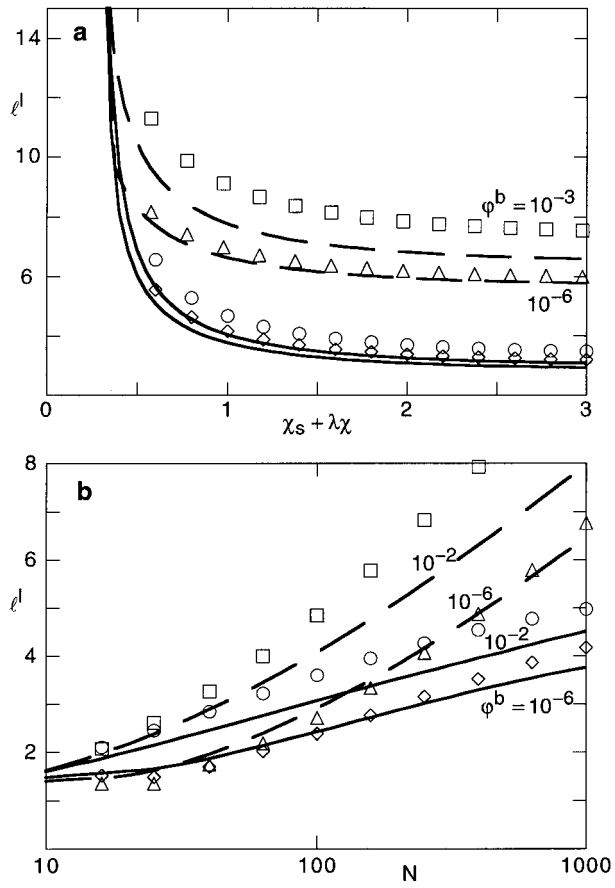

Figure 12. As Figure 11, but now for the average loop length. In (b) the highest concentration (with the longest loops) is $\varphi^b = 10^{-2}$ instead of 10^{-3}.

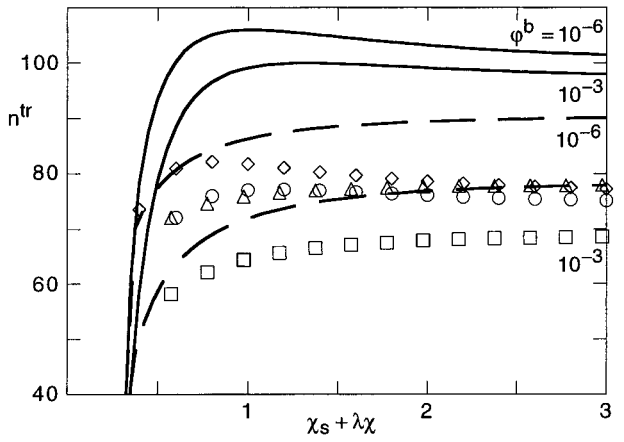

Figure 13. Number of trains (or loops) per chain as a function of $\chi_s + \lambda\chi$, for $N = 10^3$ and $\varphi^b = 10^{-6}$ and 10^{-3}. The solid and dashed curves are numerical results for $\chi = 0$ and $\chi = 0.5$, respectively. Symbols are the plateau approximation.

easily understood by realizing that, according to eqs 19a and 19b, $l^l/l^{tr} = \nu^l/\nu^{tr} = \Gamma^l/\Gamma^{tr}$. Hence, at high χ_s in a good solvent $l^l < l^{tr}$, because then $\Gamma^l < \Gamma^{tr}$ (see Figure 3), and $l^l > l^{tr}$ in a Θ solvent where loops have a higher (and chain length dependent) contribution. With decreasing χ_s, Γ^{tr} (Figure 2a) decreases more strongly than Γ^l (Figure 3a), and the ratio Γ^l/Γ^{tr} increases more strongly with decreasing χ_s than l^{tr} (Figure 9a) so that l^l increases whereas l^{tr} decreases. At very small $\Delta\chi_s$, in the Henry region, $l^l = \lambda^{-1}(\Gamma^l/\Gamma^{tr})(g_1/g_2) = \lambda^{-1}((d_h/2)e^{-1/d_h})e^{1/d_h} = d_h/2\lambda$, which diverges for $\chi_s \rightarrow \chi_{sc}$ (see Figure I-5). Hence, in the Henry region the average loop length is directly related to d_h.

In Figure 12b the loop length is shown as a function of N. This plot has the same features as Figure 3b: $l^l \propto (\Gamma^l/\Gamma^{tr})(l^{tr} - 1) \propto \Gamma^l$, since Γ^{tr} and l^{tr} are constant for high N. Hence, the loop length approaches a constant level (around 5) in a good solvent and increases with log N in a Θ solvent, just as is observed for the adsorbed amount in loops.

Figure 13 gives some information about the number of trains (and loops) per adsorbed chain. According to eq 20a n^{tr} varies as g_1g_2/Γ, where the product g_1g_2 is basically only a function of χ_s. The variation of $\Gamma = \Gamma^{tr} + \Gamma^l + \Gamma^t$ with N and φ^b has been shown in Figures 3−5. Therefore, we illustrate here only how n^{tr} depends on χ_s (Figure 13). This dependence can be understood from the second form of eq 20a in combination with eq 20b: $n^{tr} \propto \nu^{tr}/(l^{tr} - 1)$. For high χ_s, both the numerator and the denominator in this expression approach a limiting value, so that n^{tr} is approximately constant. In a good solvent, there are slightly more trains than in a Θ solvent. For $\chi = 0$, n^{tr} increases slightly with decreasing χ_s, and for $\chi = 0.5$ a weak decrease is observed. These trends are present in both the analytical and numerical models. As χ_s approaches χ_{sc}, the number of trains (and loops) decreases rapidly as the chains adopt a looser structure, with fewer (but longer) loops and longer tails.

Figure 14 shows the average tail length l^t as a function of the adsorption energy (Figure 14a), the chain length (Figure 14b), and the bulk concentration (Figure 14c). The general shape of $l^t(\chi_s)$, as given in Figure 14a, resembles that of the loop length l^l (Figure 12a). For high χ_s, there is only a weak dependence on the adsorption energy, with l^t increasing slightly with decreasing χ_s on account of the decrease of the numerators in eq 23 with increasing proximal length p. Tails are longer in a Θ solvent, the more so as the chain length increases. For both a good solvent and a Θ solvent, the tail length is approximately proportional to $y^{-2} = 1/\ln(1/\varphi^b)$, giving tails which are longer by a factor of 2 for $\varphi^b = 10^{-3}$ as compared to 10^{-6}. For χ_s approaching χ_{sc}, very long tails develop as close to χ_{sc} the chains transform into fluffy pancakes.

Figure 14b demonstrates that l^t is roughly proportional to the chain length N, as expected from eq 23. Again, tails are longer in more concentrated solutions (in this case the ratio is $\ln(10^6)/\ln(10^4) = 1.5$), and they are longer in a Θ solvent. Finally, Figure 14c gives more detail about the relative tail length l^t/N as a function of the concentration. The approximate proportionality with y^{-2} is corroborated, with only minor deviations for long chains ($N = 10^3$) in concentrated solutions (close to 10^{-2}), which is to be expected. In this figure, we show only the coupled analytical solution; for $N = 1000$ this is very close to the uncoupled plateau approximation, but for the shorter chains ($N = 100$) the uncoupled solution is about a factor of 2 too high in dilute solutions.

As our last example in this section, we show in Figure 15 the number n^t of tails per chain as a function of χ_s (Figure 15a) and N (Figure 15b). According to eq 22a n^t is proportional to $1 - \alpha\nu^{tr}$, where α depends only (weakly) on N. In a good solvent, with a small loop contribution, ν^{tr} is relatively high and, consequently, n^t is small: on average slightly above one tail per chain develops at high χ_s. In a Θ solvent ν^{tr} is smaller and n^t closer to 2. With decreasing χ_s the number of tails per chain gradually increases, to reach the limit $n^t = 2$ at the critical adsorption energy χ_{sc}.

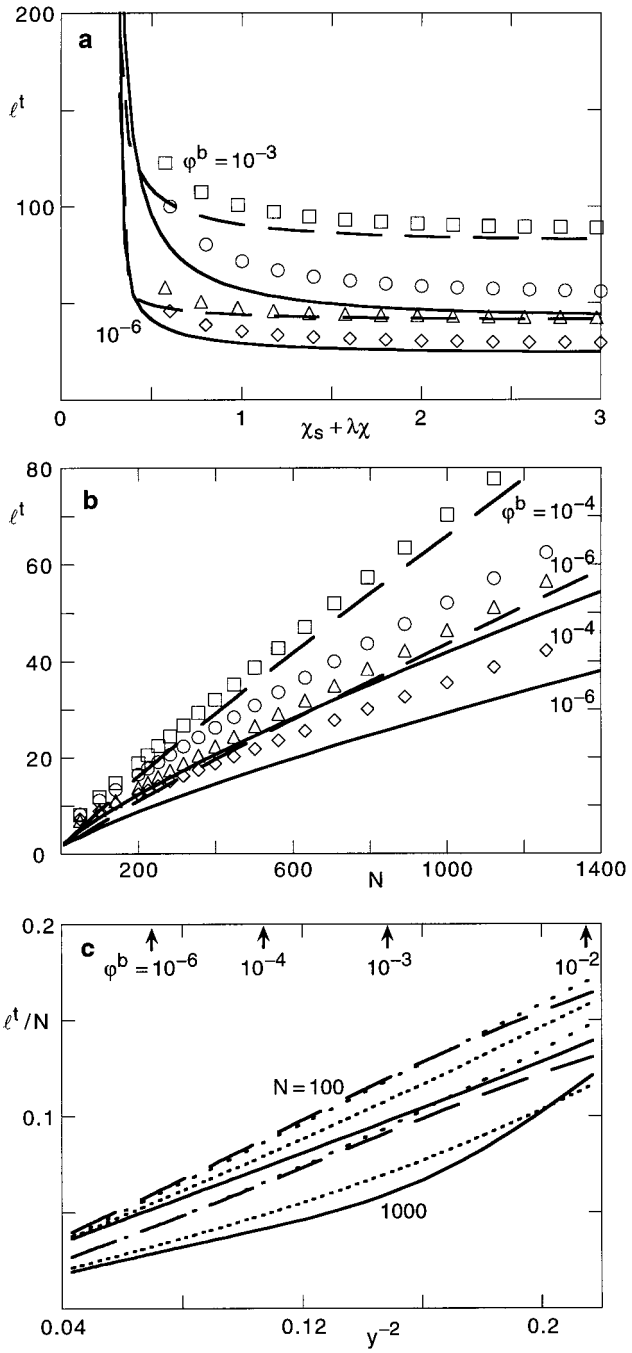

Figure 14. Average tail length as a function of $\chi_s + \lambda\chi$ (for $N = 10^3$ and $\varphi^b = 10^{-6}$ and 10^{-3}) (a), as a function of N (for $\chi_s = 1$ and $\varphi^b = 10^{-6}$ and 10^{-4}) (b), and the relative tail length l^t/N as a function of y^{-2} (for $\chi_s = 1$ and $N = 100$ and 1000) (c). The solid and dashed curves are numerical results for $\chi = 0$ and $\chi = 0.5$, respectively. In (a) and (b), the symbols represent the plateau approximation. In (c) the dotted curves give the results of the coupled approximation.

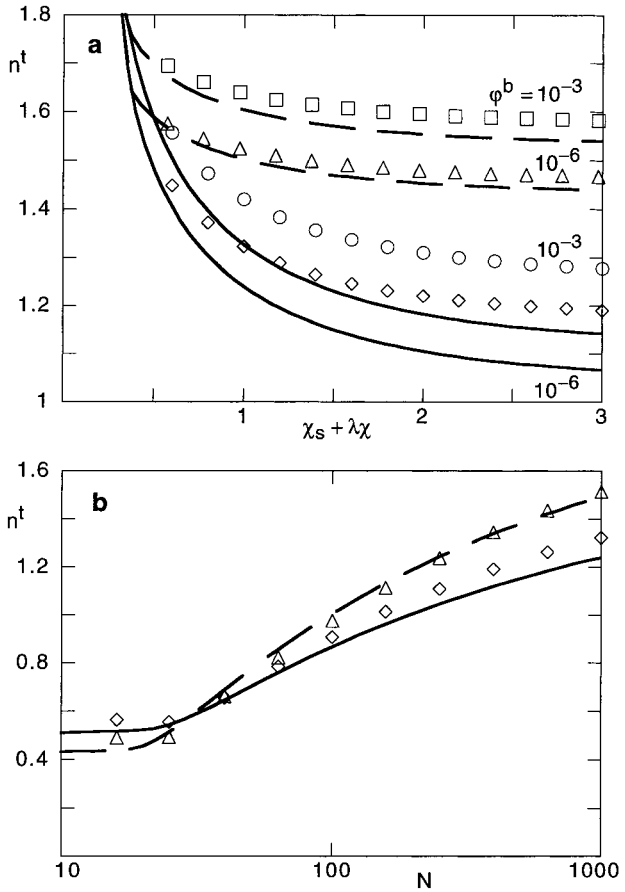

Figure 15. Average number of tails per chain as a function of $\chi_s + \lambda\chi$ (for $N = 10^3$ and $\varphi^b = 10^{-6}$ and 10^{-3}) (a) and as a function of N (for $\chi_s = 1$ and $\varphi^b = 10^{-6}$) (b). The solid and dashed curves are numerical results for $\chi = 0$ and $\chi = 0.5$, respectively. Symbols represent the plateau approximation.

Figure 15b shows how n^t depends on the chain length for given φ^b and χ_s. For very short chains (in the Henry region) there is, on average, only one tail per two chains. This follows also from the equations derived in part I for the Henry region. It is easily shown that $n^t = 2bl_g/\Gamma$ in the Henry regime leads to $n^t = 2d_h e^{-1/2d_h}/(1 + d_h e^{-1/2d_h})$. For $\chi_s = 1$ and $\chi = 0$, $d_h = 0.76$, which gives $n^t = 0.56$, in complete agreement with Figure 15b. For longer chains there is a gradual increase of n^t toward a final level. In a good solvent this level is below 2 since $\nu^{tr} = \Gamma^{tr}/\Gamma$ remains relatively high. In a Θ solvent Γ continues to increase with N (Figure 3b) so that ν^{tr} becomes very small and n^t then approaches 2.

3.4. Train, Loop, and Tail Size Distribution. In section 2.5 we derived some analytical approximations for the size distribution of trains and loops. For the tail size distribution, we have only a rather complicated analytical result for a good solvent (eq AI-7). In this last section we compare these results with the numerical data. Because the average train, loop, and tail lengths were discussed extensively in the previous section, we concentrate here on the distribution around the average.

For trains this is relatively simple. According to eq 25, the fraction of trains of given length s can be expressed in terms of l^{tr} only:

$$\ln(l^{tr} f^{tr}(s)) = (s-1)\ln\left(1 - \frac{1}{l^{tr}}\right) \approx -\frac{s-1}{l^{tr}} \quad (29)$$

where the last approximation is valid when $1/l^{tr}$ is small enough. Consequently, a semilogarithmic plot of $l^{tr}f^{tr}$ against the reduced train length s/l^{tr} should give a straight line. In order to make this plot (nearly) universal (i.e., independent of the value of l^{tr}), we choose to plot $l^{tr}f^{tr}$ as a function of $(s-1)/l^{tr}$. Figure 16 gives the numerical results for $N = 1000$, $\varphi^b = 10^{-6}$, and $\chi_s = 1$ plotted in this way, for both a good solvent and a Θ solvent. The nearly exponential distribution is nicely corroborated, and the two curves approximately coincide. According to eq 29 the slope of this plot should equal $l^{tr}\ln(1 - 1/l^{tr})$, which is close to −1. For $\chi = 0$ in

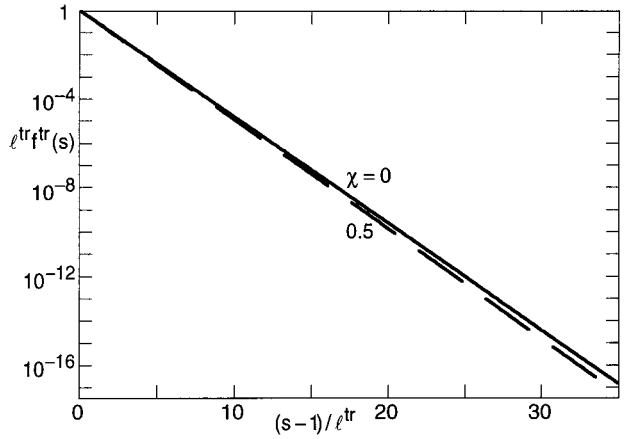

Figure 16. Numerical train size distribution for $N = 10^3$, $\chi_s = 1$, and $\varphi^b = 10^{-6}$. The fraction $f^{tr}(s)$ of trains with length s is normalized by l^{tr} (see eq 29) to represent the spread around the average.

Figure 16 $l^{tr} = 5.37$ (Figure 11), which should correspond to a slope of -1.107. This is exactly the slope found in Figure 16. For $\chi = 0.5$, l^{tr} is smaller, leading to a slightly higher slope. We conclude that the distribution of the train sizes around their average is very accurately predicted by eq 25 (or eq 29), which equation is identical to the random-walk result of Hoeve et al.[8,9] The reason for this nice agreement is that walks in the surface layer take place in a uniform field. The magnitude of this field (and that in the second layer) determines the average train length, but the spread around this average can be obtained from random-walk statistics because each step in the surface layer has the same weight.

The expression for the loop size distribution is more complicated as the loops segments experience a nonuniform field which, moreover, is weaker in a Θ solvent as compared to a good solvent. According to eq 26, the loop size distribution $n^l(s)$ can be written as $N - s$ times $W^l(s) = G^t_{2,s}e^{-\epsilon s}$. The full equation for $W^l(s)$ in a good solvent is given in eq AI-7; its limiting form for long chains (small $1/d$) is presented in eq 27. For large s, $G^t_{2,s}$ can be approximated as the power law $G^t_{2,s} \propto s^{-5/2}$. In a Θ solvent a power law s^{-2} is expected for $n^l(s)$. Therefore, we present the data for $G^t_{2,s}$ and $f^l(s) = n^l(s)/n^l$ in a double-logarithmic plot (Figure 17a,b). Figure 17c replots the data of Figure 17b with a linear scale for s; this form would give a straight line if $f^l(s)$ would be an exponential function of s.

Figure 17a shows the numerical data for $G^t_{2,s}$ and the analytical result $W^l(s)e^{\epsilon s}$ for $N = 1000$, $\varphi^b = 10^{-6}$, and $\chi_s = 1$. The numerical data are given again as solid and dashed curves, the analytical result for $\chi = 0$ (eq AI-7) as the dotted curve, and the expanded version (eq 27) as symbols. The analytical result was normalized such that $G^t_{2,1}$ equals G_2 (according to the numerical model). For the relatively short chain length of Figure 17 (where $d \approx 4.6$), the expanded form in eq 27 still deviates from the full equation AI-7. For higher values of d, eqs 27 and AI-7 become nearly identical (not shown here).

For the good solvent a comparison between analytical and numerical results is possible. The agreement is excellent for short loops, which are the most abundant anyhow. For long loops the analytical decay is somewhat slower than the numerical one, which is probably due to the inaccurate field used in the analytical model,

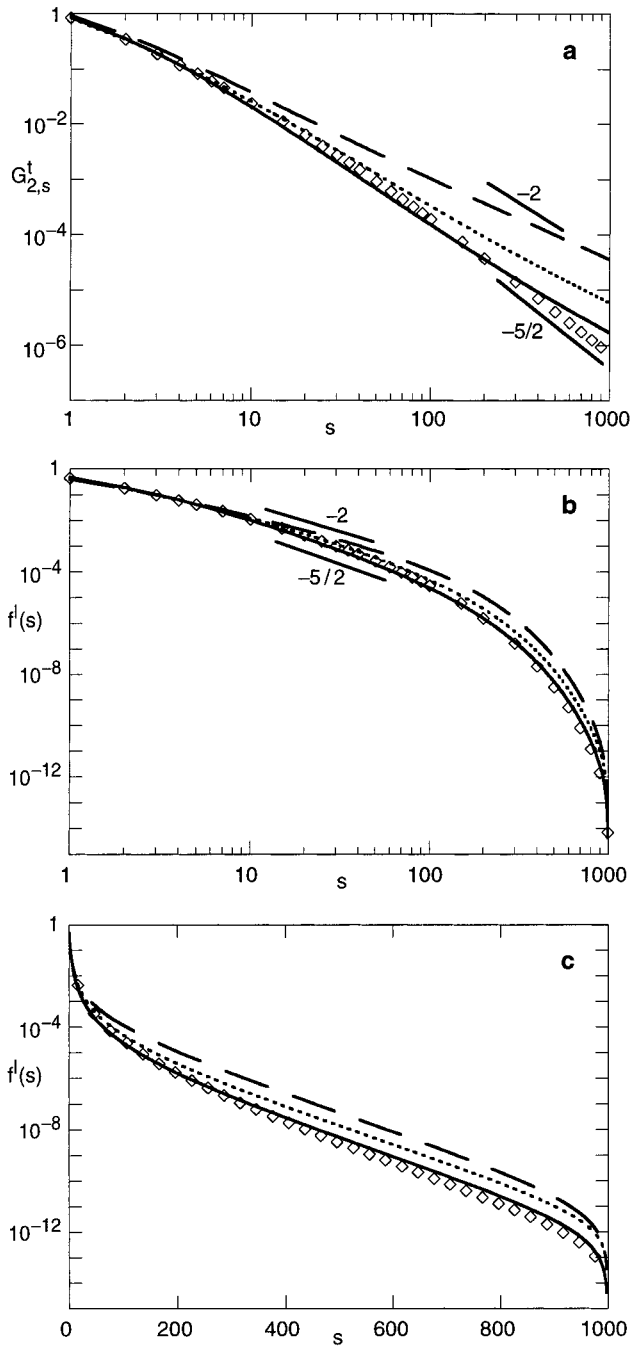

Figure 17. Distribution $G^t_{2,s}$ for walks returning to the second layer (a) and the loop size distribution, for $N = 10^3$, $\chi_s = 1$, and $\varphi^b = 10^{-6}$. The fraction $f^l(s)$ of loops with length s is plotted both with a logarithmic (b) and a linear (c) scale for s. The solid and dashed curves are numerical results for $\chi = 0$ and $\chi = 0.5$, respectively. The dotted curves represent the full analytical solutions for $\chi = 0$ according to eq AI-7 ($G^t_{2,s}$). Symbols represent the expanded form of $G^t_{2,s}$ (eq 27). The expected scaling dependencies are indicated.

where the contribution of tails was neglected. Overall the agreement is quite satisfactory, and it is expected to be even better for longer chains. For long loops $G^t_{2,s}$ approximately follows a power law. The apparent scaling exponent for the analytical result is smaller than for the numerical one, and for these rather short chains both are below the limiting value $^5/_2$ expected for long chains.

For $\chi = 0.5$ no analytical result is available and we give only the numerical result for $G^t_{2,s}$ (dashed). The

decay of $G^t_{2,s}$ with s is slower than in a good solvent (because the field is smaller in a Θ solvent). For high s again an approximate power law is followed, with an exponent which for $N = 10^3$ is smaller than the scaling prediction -2 for $n^l(s)$ for long chains.

Figure 17b,c gives the size distribution, expressed as the fraction $f^l(s)$ of the total number of loops which is of size s. In this presentation we do not have to worry about any normalization constant. From eq 26 it is clear that $f^l(s)$ should be proportional to $N - s$ times $W^l(s) = G^t_{2,s}e^{-\epsilon s}$. Scaling predicts $f^l(s)$ to be a power law; if that were the only effect, a double-logarithmic plot (Figure 17b) should be a straight line. The analytical result gives a power law for $G^t_{2,s}$ (for high s), but the additional factors $(N - s)e^{-\epsilon s} \approx Ne^{-(\epsilon+1/N)s}$ (for $s << N$) gives an exponential dependence as well. If the latter would be the main effect, a semilogarithmic plot of $f^l(s)$ (Figure 17c) would give a straight line. Both features are to some extent obeyed. In Figure 17b there is a region where the power law seems to be valid (with an exponent which is close to the scaling prediction). However, for long loops the exponential dependence seems to be followed over a rather wide range (Figure 17c).

At any rate, it is gratifying to note that for $\chi = 0$, for which an analytical result is available, the agreement between analytics (dotted curves) and numerics (solid curves) is rather good over the entire range of s, from $s = 1$ to $s = N$. This agreement is expected to become even better for longer chains, for which probably also the power-law region would be wider.

For $\chi = 0.5$ there is no analytical result, and we can compare the numerical data for $f^l(s)$ (long dashes in Figure 17b,c) only with the scaling predictions. Indeed, the power-law exponent is smaller in a Θ solvent, and the agreement in Figure 17b is of the same level as for $\chi = 0$.

Figure 18 gives similar information as Figure 17, but now for the tail size distribution. In Figure 18a the numerical result for $G^f_{2,s}$ is given (for both $\chi = 0$ and $\chi = 0.5$). The dotted curve shows $e^{\epsilon s}\sum_z W^t(z,s)$ (see eq 28) for $\chi = 0$ according to eq AI-7. The latter result was again normalized by requiring equality for $s = 1$. As expected, $G^f_{2,s}$ for tails (Figure 18a) decays much slower than $G^t_{2,s}$ for loops (Figure 17a). The agreement between numerics and analytics is quite reasonable, considering the fact that the tails find themselves predominantly in a field which is systematically underestimated by $u = g^2$. There is an approximate power-law decay, but the apparent exponents are smaller than the ones predicted by scaling (for $n^t(s)$). For a good solvent the numerical decay is closer to the scaling prediction than the analytical result.

The numerical tail size distributions $f^t(s) = n^t(s)/n^t$ are shown in Figure 18b,c. For these there is very good agreement between the analytical and numerical models (for $\chi = 0$). In this parameter set, there is also not much difference between a good and a Θ solvent; however, the two curves in Figure 18b cross each other. For relatively short tails, an approximate power-law behavior is found, with exponents that are close to the scaling predictions (Figure 18b). As shown in Figure 18c, very long tails are better described by an exponential decay: for large s the exponential factor $e^{-\epsilon s}$ dominates.

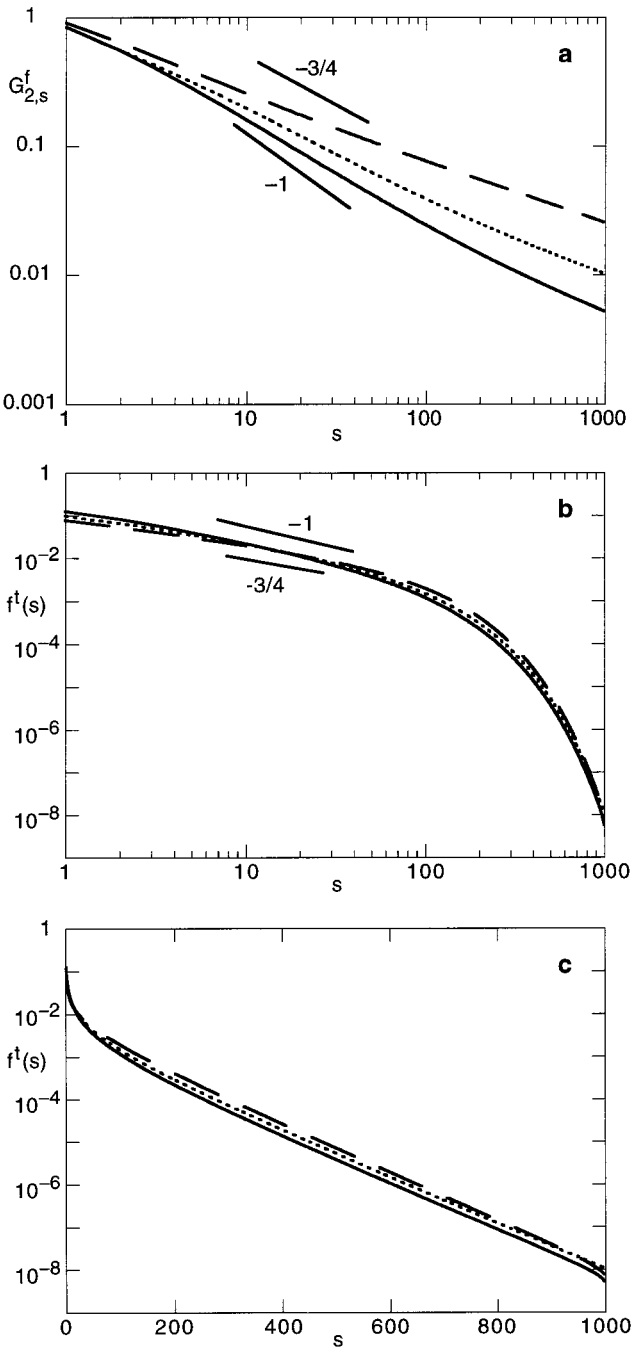

Figure 18. Distribution $G^f_{2,s}$ for free walks starting in layer 2 (a) and the tail size distribution (b, c), for $N = 10^3$, $\chi_s = 1$, and $\varphi^b = 10^{-6}$. As in Figure 17, the fraction $f^t(s)$ of tails with length s is plotted both with a logarithmic (b) and a linear (c) scale for s. The solid and dashed curves are numerical results for $\chi = 0$ and $\chi = 0.5$, respectively. The dotted curves represent the analytical solutions according to eq AI-7. The expected scaling dependencies are indicated.

4. Concluding Remarks

We presented a detailed study of the adsorption layer structure using an analytical approximation to the numerical mean-field lattice model of Scheutjens and Fleer. The analytical approach is based upon a recent mean-field theory proposed by Semenov et al., which goes one step beyond the ground-state approximation. In the original theory of Semenov et al. there are two characteristic mesoscopic length scales: a characteristic distance z^* separating an inner layer made up by loops and an outer layer built up by tails, and a cutoff length

d which is the radius of gyration divided by a factor related to the solution concentration. In the asymptotic limit of extremely long chains, d is indeed the largest scale and the two length scales are well separated. However, for moderate chain lengths and high dilution the opposite holds. Over most of the (dilute) concentration range (typically $\varphi^b < 10^{-3}$) and chain-length range (typically $N < 10^4$) covered in this paper, we check that the cutoff length d is shorter than z^* and that the numerical results can be accurately described by a theory based on the cutoff (or distal) length and a proximal length. The latter is determined by the monomer−wall interaction and is found from a boundary condition derived from the lattice model. Physically, the fact that z^* does not enter means that the tail monomers only dominate in the dilute edge, where the structure is imposed by the bulk chemical potential anyhow. This does not imply, however, that tails play no role whatsoever. Tails double the layer thickness and tail monomers dominate over loop monomers in a significant part of the adsorbed layer.

A large number of structural details are calculated, including the position and height of the tail maximum and the size distributions of trains, tails, and loops. The train size distribution shows clearly that in the plateau of the adsorption isotherm the train size is nearly independent of the chain length and is small: typically around 5. This might have interesting implications for the kinetics. One could speculate that in the plateau regime chains should be fairly reversibly adsorbed in most cases, as train desorption remains easy. On the other hand, in the early, very starved stages of the adsorption process trains are very long and difficult to desorb. In order to reach the equilibrium plateau adsorption, starting from an extremely dilute solution and a bare surface should then be avoided. A way to reach quick equilibrium might be to let the long chain one wants to adsorb compete for the surface with many short chains. The latter are expected to cover and protect the surface in the early stages and to be displaced by the long chains afterward.[12−14]

The loop and tail size distributions obtained analytically are in excellent agreement with the numerics. These distributions are markedly different from early zero-field predictions by Hoeve,[8,9] as is to be expected from scaling arguments (see Appendix II). Formally the scaling results (transposed to mean field) are contained in our results. Nevertheless, the expected power law does not describe a significant part of the layer for the (relatively short) chains considered in this paper.

The adsorbance in trains, loops, and tails is calculated as a function of the chain length, the bulk concentration, and the surface affinity of the monomers. Good agreement with the numerical data is obtained. The analytics give systematically slightly lower values, mainly due to the loop contribution. This stems from an overestimation (as compared to the lattice calculation) of the molecular field in the steep profile region close to the wall. This effect is more pronounced in a Θ solvent.

Both the numerics and the analytics presented in this paper are limited to mean-field and thus to so-called marginal solvents where the chains remain almost Gaussian. Hence, our computations for $\chi = 0.5$ may be expected to describe the adsorption of real chains from a Θ solvent reasonably well. Those for $\chi = 0$ are more dubious since chain swelling was neglected. This swelling is expected to occur for chains or chain sections for which $v\sqrt{n}$ exceeds unity, where n is the length of the chain (section). Hence, for $\chi = 0$ ($v = 1$) swelling occurs at all scales. However, for most experimental good solvents ($v = 0.1-0.2$) swelling is only important for n larger than $O(10^2)$. Since the average tail length is at least an order of magnitude smaller than the chain length (see eq 23 and Figure 14), under most conditions the adsorbed layer is then correctly described by the present treatment. Obviously, this does not apply to the bulk solution when $N >> 10^2$: swelling affects the chemical potential. In the limit of asymptotically long chains, it is rather easy to correct for this by renormalizing the bulk concentration. To that end, the equation for the end-point distribution (eq I-8) has to be replaced by the more general expression $\varphi_z^{ae}/\varphi_\infty^e = G_{z,N}^a/G_{\infty,N}$, where now $G_{\infty,N} \neq 1$. In order to account for chain swelling, it is thus enough to replace φ_{MF}^b by $\varphi_{SA}^b/G_{\infty,N}$ (MF = mean field, SA = self-avoiding), and all our results remain valid. Our calculations for a given value of φ_{MF}^b then apply to a concentration φ_{SA}^b ($=\varphi_{MF}^b G_{\infty,N}$) of swollen chains.

In the asymptotic limit of long self-avoiding walks with $v = 1$ it has been found that $G_{\infty,N} \approx (\lambda\mu)^N N^{\gamma-1}$, where γ (= 1.16) is a critical exponent and $1/\mu$ ($>\lambda$) an "effective lattice parameter".[15] Swelling thus reduces the partition function by a nearly exponential factor, the additional enhancement factor $N^{\gamma-1}$ being only a small correction. For a simple cubic lattice $\lambda\mu = 0.7806$, and for a hexagonal lattice $\lambda\mu = 0.7198$,[15] which would imply a huge renormalization factor for $v = 1$ and large N. We are, however, concerned with weakly repulsive interactions (v around 0.1), when the bulk chains are not self-avoiding at all scales. We are not aware of any explicit expression for the partition function of a lattice chain with weak monomer/monomer repulsion.[16] Defining a minimal size $g = 1/v^2$ for self-avoidance to be relevant, we may interpolate for $1 << g << N$ by a scaling law $G_{\infty,N} \approx (\lambda\mu)^{N/g}(N/g)^{\gamma-1}$. For a typical situation of $N = 10^3$, $\lambda = {}^1/_6$, and $v = 0.1$ ($\chi = 0.45$), this would imply a renormalization factor of about 10: our mean-field calculations for, say, $\varphi^b = 10^{-6}$, would then describe the adsorption of real (partially swollen) chains at a concentration of around 10^{-7}.

For very long chains and/or better solvents, the tails are swollen but the loops may still be marginal. The layer would then split in an inner marginal layer and an outer excluded-volume layer. The quantitative description of such a layer goes beyond the scope of the present work.

Appendix I. Loop and Tail Size Distribution in a Good Solvent

In this appendix we calculate the statistical weight of configurations that start in the second layer and do not penetrate into the train layer (hence, we consider G^f). In the lattice model, where z and s are positive integers, the statistical weight for free walks starting with segment 1 in z' and ending with s in z may be denoted as $G_{z,s|z',1}^f$. This function satisfies the propagator relation I-3 in paper I. For loops and tails $z' = 2$. The function $G_{2,s}^t$ in eq 26 equals $G_{2,s|2,1}^f$, and $G_{2,s}^f$ in eq 28 is an abbreviation for the sum of $G_{z,s}^t = G_{z,s|2,1}^f$ over $z = 2, 3, \ldots$. Analogously to eq I-3 the starting condition for computing $G_{z,s|z',1}^f$ is $G_{z,1|z',1}^f = e^{-u_z}\delta(z - z')$ or, equivalently, $G_{z,0|z',0}^f = \delta(z - z')$; moreover, $G_{1,s|z',1}^f = 0$ since the train layer is forbidden.

In the continuum description we try to find $G^f(z,s|z',0)$, where $z' = {}^3/_2$ for loops and tails, with boundary conditions $G^f(1,s|z',0) = 0$ (since the region $z < 1$ is forbidden for free walks), and again $G^f(z,0|z',0) = \delta(z - z')$. The discrete propagator relation is now replaced by the differential equation $\lambda\, \partial^2 G^f/\partial z^2 = \partial G^f/\partial s + uG^f$ (see eq I-11).

It turns out that it is more convenient to find the function $W(z,z',s) = G^f(z,s|z',0)e^{-\epsilon s}$, which directly enters the size distributions (eqs 26 and 28). The exponential cutoff allows to neglect tails in the field u. In terms of W, the loop size distribution (eq 26) is proportional to $(N - s)W({}^3/_2,{}^3/_2,s)$ and the tail size distribution to the integral of $W(z,{}^3/_2,s)$ over the region $z > 1$. In the main text we abbreviated $W({}^3/_2,{}^3/_2,s)$ as $W^l(s)$, and $W(z,{}^3/_2,s)$ as $W^t(z,s)$.

Inserting W into the differential equation gives

$$-\frac{\partial W}{\partial s} = -\lambda\frac{\partial^2 W}{\partial z^2} + (g^2 + \epsilon)W \qquad \text{(AI-1)}$$

where as before we use $u = g^2$, thereby neglecting the tail contribution to the field. In a good solvent we have $g^2 = 2\epsilon/\sinh^2 x$, with $\epsilon = \lambda/d^2$ and $x = (z + p)/d$. If we introduce a reduced monomer index $n = \epsilon s$, eq AI-1 simplifies to

$$-\frac{\partial W}{\partial n} = -\frac{\partial^2 W}{\partial x^2} + \left(\frac{2}{\sinh^2 x} + 1\right)W \qquad \text{(AI-2)}$$

which after Laplace transformation reads

$$-rW + \delta(x - x') = -\frac{d^2 W}{dx^2} + \left(\frac{2}{\sinh^2 x} + 1\right)W \qquad \text{(AI-3)}$$

where r is the Laplace variable associated with n, and where we used the boundary condition $W(x,x',0) = \delta(x - x')$. For $x \neq x'$ this equation reduces to

$$\frac{d^2 W}{dx^2} = \left(\frac{2}{\sinh^2 x} + 1 + r\right)W \qquad \text{(AI-4)}$$

with $W(x_2,x',r) = 0$, where $x^2 = (p + 1)/d$ according to eq 3. The δ function introduces a cusp singularity at $x = x'$, with $[dW/dx]_{x'-}^{x'+} = -1$. The general solution of eq A1-4 is of the form

$$W(x,x',r) = A(x',r)e^{\omega(x-x_2)}(\omega - \coth x) + B(x',r)e^{\omega(x-x_2)}(\omega + \coth x)$$

where $\omega^2 = 1 + r$, and A and B are fixed by the boundary conditions. After determining A and B on either side of the singularity, $W(x,x',r)$ can be expressed in closed form as

$$W(x,x',\omega) = \frac{1}{\omega(1-\omega^2)}\left\{\frac{\omega - \coth x_2}{\omega + \coth x_2}(\omega + \coth x) \times (\omega + \coth x')e^{-\omega(x+x'-2x_2)} - (\omega - \coth x_s)(\omega + \coth x_l)e^{-\omega|x-x'|}\right\} \qquad \text{(AI-5)}$$

with x_s the smallest value of the pair x,x' and x_l the largest.

This Laplace transform can be written as a sum of simple terms, each of which can be inverted. The inverse Laplace transform of $e^{-\omega k}/(\omega + \alpha)$ is

$$f(k,\alpha,n) = \left\{\frac{1}{\sqrt{\pi n}}\exp\left(-\frac{k^2}{4n}\right) - \alpha e^{\alpha k}e^{\alpha^2 n} \times \operatorname{erfc}\left(\alpha\sqrt{n} + \frac{k}{2\sqrt{n}}\right)\right\}e^{-n} \qquad \text{(AI-6)}$$

where erfc x is the complementary error function. We use the following abbreviations:

$$B = \coth x_2, \quad x_+ = x + x' - 2x_2, \quad x_- = |x - x'|, \quad C_s = \coth x_s, \quad C_l = \coth x_l, \quad C = \coth x, \quad C' = \coth x'$$

The solution is now

$$W(x,x',s) = G^f(x,x',s)e^{-\epsilon s} = -\frac{CC'}{2}f(x_+,0,\epsilon s) + \frac{C_sC_l}{2}f(x_-,0,\epsilon s) - \frac{(B - C)(B - C')}{B^2 - 1}f(x_+,B,\epsilon s) + \frac{B - 1}{4(B + 1)}(C + 1)(C' + 1)f(x_+,-1,\epsilon s) + \frac{B + 1}{4(B - 1)}(C - 1)(C' - 1)f(x_+,1,\epsilon s) - \frac{(C_s - 1)(C_l + 1)}{4}f(x_-,-1,\epsilon s) - \frac{(C_l - 1)(C_s + 1)}{4} \times f(x_-,1,\epsilon s) \qquad \text{(AI-7)}$$

The loop size distribution involves $W^l(s) = W(x_3,x_3,s)$, where $x_3 = (p + {}^3/_2)/d$, so that in the above equations x_+ reduces to $1/d$ and x_- to zero. In this case all C's are equal to coth x_3. The sum of the first two terms reduces to $(C^2/\sqrt{4\pi\epsilon s})(1 - e^{-1/4\lambda s})$. If $G^f(x_3,x_3,s) = G^t_{2,s}$ is then expanded in terms of $1/d = \sqrt{\epsilon/\lambda}$ to lowest order, eq 27 in the main text is obtained.

For the tail size distribution we need the integral of $W^t(z,s) = W(x,x_3,s)$ from $x = x_2$ to infinity. Unfortunately, most of the integrals cannot be expressed in the form of tabulated functions. For a given value of x, an expansion of the type leading to eq 27 is possible, but also this expression cannot be integrated analytically. For the computation of the tail size distribution in Figure 18 from eq AI-7, we discretized the equation by calculating the sum of $W^t(z,s)$ over the values at $z = {}^3/_2$, ${}^5/_2$, ...

Appendix II. Scaling Description of the Loop and Tail Size Distribution

We summarize the arguments proposed by Bouchaud and Daoud[10] and De Gennes.[11]

A. Loops. The overall concentration profile follows the scaling law $\varphi \approx z^{-\alpha}$, where in our mean-field picture $\alpha = 2$ in a good solvent and $\alpha = 1$ in a Θ solvent. This profile can be considered to be made up of loops of various sizes (we neglect the contribution of tails).

A typical loop of s segments reaches a distance $z \approx s^\nu$, where ν is the scaling exponent for the radius of gyration ($R \propto N^\nu$); in our mean-field description we have ideal chains with $\nu = {}^1/_2$ in both a good and a Θ solvent. We have $n^l(s)$ ds loops of size between s and $s + ds$. We may also define a cumulative size distribution $N^l(s) =$

$\int_s^\infty n^l(s')\,ds'$, giving the number of loops with a size larger than s. Clearly, $n^l(s) = -dN^l/ds$.

Now consider the total number of segments within a distance z from the surface. All loops smaller than $z^{1/\nu}$ lie within z and contribute s segments. This total contribution of small loops is $\int_0^{s'} s n^l(s)\,ds$, where $s' = z^{1/\nu}$. Big loops ($s > s' = z^{1/\nu}$) have s' segments within z and the remainder outside. Hence, the total number of segments within z is given by

$$\int_0^z \varphi(z')\,dz' = \int_0^{z^{1/\nu}} s n^l(s)\,ds + z^{1/\nu}\int_{z^{1/\nu}}^\infty n^l(s)\,ds \qquad \text{(AII-1)}$$

Differentiation of this equation with respect to z gives

$$\varphi(z) = \frac{1}{\nu} z^{1/\nu - 1}\int_{z^{1/\nu}}^\infty n^l(s)\,ds \quad \text{or}$$

$$N^l(s) = \nu z^{1-1/\nu}\varphi(z) = \nu z^{1-1/\nu-\alpha} \qquad \text{(AII-2a,b)}$$

Substitution of $z \approx s^\nu$ in the latter equation gives an explicit expression for the cumulative distribution, and $n^l(s) = -dN^l/ds$ gives the loop size distribution as

$$n^l(s) \propto s^{-(2-\nu+\alpha\nu)} \qquad \text{(AII-3)}$$

For a good solvent $\alpha = 2$ and $\nu = {}^1/_2$ (mean field), so that $n^l(s) \propto s^{-5/2}$; for a Θ solvent $\alpha = 1$ and $\nu = {}^1/_2$ so that $n^l(s) \propto s^{-2}$.

B. Tails. The number of end points in between z and $z + dz$ equals $\varphi^e(z)\,dz$, and it is also given by $n^t(s)\,ds$, where again z and s are coupled through $z \approx s^\nu$ because, as for loops, tails of s segments can reach a distance z^ν. Hence, $n^t(s) = \varphi^e(z)(dz/ds) = \nu\varphi^e(z)s^{\nu-1}$. The end-point concentration φ^e scales as $z^{-\alpha/2}$ because $\varphi^e \propto g \propto \varphi^{1/2}$. Hence $\varphi^e \propto z^{-\alpha/2} = s^{-\alpha\nu/2}$, and we find for the tail size distribution

$$n^t(s) \propto s^{-(1-\nu+\alpha\nu/2)} \qquad \text{(AII-4)}$$

For a good solvent ($\alpha = 2$, $\nu = {}^1/_2$) this gives $n^t(s) \propto s^{-1}$, whereas for a Θ solvent ($\alpha = 1$, $\nu = {}^1/_2$) we have $n^t(s) \propto s^{-3/4}$.

Appendix III. List of Most Important Symbols

Most of the symbols are the same as in part I (see Appendix I of part I). A few additional symbols occurring in part II (excluding those used only in Appendices I and II) are listed below. In this paper p and d are in most cases p_p and d_p, as used in part I.

$f^x(s)$	fraction of sequences x with s segments: $f^x(s) = n^x(s)/n^x$ (x = tr, l, t)
$G^t_{z,s}$	statistical weigth of tails of length s ending in z
$G^t_{2,s}$	statistical weigth of loops of length s (a loop is a tail returning to layer 2)
n^x	number of trains (x = tr), loops (x = l), or tails (x = t) per adsorbed chain
$n^x(s)$	number of sequences x of length s per adsorbed chain
$W^l(s)$	$e^{-\epsilon s}G^t_{2,s}$ (eq 26)
$W^t(z,s)$	$e^{-\epsilon s}G^t_{z,s}$ (eq 28)
x_l	value of x where $\varphi^l = \varphi^b$
x_m	value of x at the maximum in the tail profile
x_t	value of x where $\varphi^t = \varphi^b$
Y	$\sqrt{y^2+2\ln b}$, as defined in eq 7; hence, $d = \sqrt{\lambda N}/Y$
z_l	value of z where $\varphi^l = \varphi^b$
z_m	value of z at the maximum in the tail profile
z_t	value of z where $\varphi^t = \varphi^b$
α	$b/g_1 \approx 1-0.15\log N$ (see eq 6 and Figure 1)
l^x	average length of sequences x (x = tr, l, t)
ν^x	average fraction of chain segments in trains (x = tr), loops (x = l), or tails (x = t)
φ_m	maximum value of $\varphi^t(z)$

References and Notes

(1) Fleer, G. J.; Van Male, J.; Johner A. *Macromolecules* **1999**, *32*, 825.
(2) Semenov, A. N.; Bonet-Avalos, J.; Johner, A.; Joanny J. F. *Macromolecules* 1**996**, *29*, 2179.
(3) Scheutjens, J. M. H. M.; Fleer G. J. *J. Phys. Chem*. **1979**, *83*, 1619.
(4) Scheutjens, J. M. H. M.; Fleer G. J. *J. Phys. Chem*. **1980**, *84*, 178.
(5) Fleer, G. J.; Cohen Stuart, M. A.; Scheutjens, J. M. H. M.; Cosgrove, T.; Vincent B. *Polymers at Interfaces*; Chapman and Hall: London, 1993.
(6) Johner, A.; Bonet-Avalos, J.; Van der Linden, C. C.; Semenov, A. N.; Joanny, J. F. *Macromolecules* **1996**, *29*, 3629.
(7) Semenov, A. N.; Joanny, J. F.; Johner, A. In *Theoretical and Mathematical Models in Polymer Research*, Grosberg, A., Ed.; Academic Press: San Diego, 1998.
(8) Hoeve, C. A. J.; DiMarzio, E. A.; Peyser, P. *J. Chem. Phys.* **1965**, *42*, 2558.
(9) Hoeve, C. A. J. *J. Chem. Phys.* **1966**, *44*, 1505.
(10) Bouchaud, E.; Daoud, M. *J. Phys. (Paris)* **1987**, *48*, 1991.
(11) De Gennes, P. G. *Adv. Colloid Interface Sci.* **1987**, *27*, 719.
(12) Fleer, G. J. *Colloids Surf. A* **1995**, *104*, 271.
(13) Baschnagel, J.; Johner, A.; Joanny, J. F. *Phys. Rev. E* **1997**, *55*, 3072.
(14) Dijt, J. C.; Cohen Stuart, M. A.; Fleer, G. J. *Macromolecules* **1994**, *27*, 3219.
(15) Des Cloizeaux, J.; Jannink, G. *Les Polymères en Solution*; Les Éditions de Physique: Les Ullys, France, 1987.
(16) *Note Added in Proof.* A recent field-theoretical analysis of very accurate Monte Carlo data (Grassberger, P.; Sutter, P.; Schaeffer, L. *J. Phys. A* **1997**, *30*, 7039) provides an accurate parametrization of the partition function for the Domb−Joyce lattice model. Though the main dependence with chain length is found to be exponential, the field-theoretical results depend upon two parameters (and not upon the Fixman parameter only as postulated in the simple scaling assumption). Excluded volume is found to be relevant for slightly shorter chains and/or slightly weaker interactions than suggested by the simple arguments given at the end of the discussion in this paper.

MA980794Q